PLOS Complex Systems

RESEARCH ARTICLE

Multi-scale local network structure critically impacts epidemic spread and interventions

Omar Eldaghar[1*], **Michael W. Mahoney**[2], **David F. Gleich**[3]

1 Department of Mathematics, Purdue University, West Lafayette, Indiana, United States of America, **2** Department of Statistics, University of California Berkeley, Berkeley, California, United States of America, **3** Department of Computer Science, Purdue University, West Lafayette, Indiana, United States of America

* oeldagha@purdue.edu

OPEN ACCESS

Citation: Eldaghar O, Mahoney MW, Gleich DF (2026) Multi-scale local network structure critically impacts epidemic spread and interventions. PLOS Complex Syst 3(9): e0000116. https://doi.org/10.1371/journal.pcsy.0000116

Editor: Jaya Sreevalsan-Nair, International Institute of Information Technology Bangalore, INDIA

Received: December 7, 2025

Accepted: June 19, 2026

Published: September 2, 2026

Data availability statement: All the experiment codes are available online at https://github.com/oeldaghar/network-epi. The full set of experiment data is contained in Zenodo directories at https://zenodo.org/records/13881920 and https://zenodo.org/records/13881977. They

Abstract

Network epidemic simulation enables fine-grained understanding of epidemic behavior. However, empirical samples of interaction networks display properties that are challenging to capture with popular synthetic models of networks. Our empirical results show that epidemic spread behavior is sensitive to a form of multi-scale local structure that is absent in common baseline models, (e.g., Erdős–Rényi, Chung-Lu, etc). This structure critically impacts the effect of local quarantining and stops epidemic spread in samples of interaction networks, even when it cannot be halted in simple synthetic models of those networks. Insights from our analysis include how epidemics on networks with widespread multi-scale local structure are easier to mitigate, as well as characterizing which nodes are ultimately not likely to be infected. We demonstrate that this structure results from more than just local triangle structure in the network, and we illustrate processes based on homophily or social influence and random walks that suggest how this multi-scale local structure arises and use it to cleanly isolate intervention sensitivity to multi-scale local structure.

Author summary

Epidemic spread is strongly dependent on the patterns and structures inherent in human contact networks. Contact patterns give rise to structural network features that can impact epidemic spread and control in complex ways. A subtle but prominent feature of real-world networks is rich multi-scale structure that manifests as groups of well-connected nodes at multiple size scales. We study this multi-scale structure and show that it can have a large impact on the control of epidemics in real networks. This structure also provides insight on what portions of the network are more resilient to infection while proving more reliable than traditional metrics such as average degree or the dominant eigenvalue. We also give generative models that reliably reproduce this structure as well

are linked in the above repository along with instructions on how to obtain the data. Note the compressed data is approximately 80GB and uncompressed it is approximately 540GB.

Funding: DFG and OE acknowledges partial NSF support from awards CCF-1909528, IIS-2007481, as well as DOE award DE-SC0023162. MWM would like to thank the ONR and NSF for partial support of this work. The funders had no role in study design, data collection and analysis, decision to publish, or preparation of the manuscript.

Competing interests: The authors have declared that no competing interests exist.

as distinguish this structure from the closing of triangles and cleanly isolate the impact of this structure on epidemic spreading.

1. Introduction and central findings

Understanding epidemic spread is fundamental to controlling, containing, and mitigating epidemic spread. Controlled experiments with epidemic spread are inherently limited to virtual pathogens, and so computational models are key to our understanding. Modeling approaches can vary over an enormous range, from models based on dynamical systems [1–3], to models fit to data [4,5], and to fine-grained event simulators that provide intricate possibilities for interventions [6–9].

A key component that is often explicit in event simulators but implicit in models based on dynamical systems is the underlying *network substrate* over which the epidemic spreads. For instance, many models (e.g., meta-population or structured dynamical systems) make use of a homogeneous mixing assumption. This amounts to assuming the underlying contact network is either an overly simplistic fully connected network (i.e., a clique) or consists of uniformly random interactions [10,11]. These assumptions are contrary to empirical work showing that these properties are not present in empirical networks [12–15]. Put plainly: network structure matters to epidemic spread and the properties of the underlying network are critical to understanding epidemic spread in empirical networks [16–18].

Our findings show that local structure at multiple size scales within a network is critical to the success or failure of local quarantine interventions. Previous studies of multi-scale structure [19, 20] are of a different type as we discuss subsequently and also focus on matching epidemic behavior instead of *intervention impact*.

Multi-scale local structure in networks

The specific gap that we address is to observe that empirically-measured networks have a rich multi-scale structure, and that this structure has important implications for interventions in epidemic spread. This structure arises empirically because individuals interact repeatedly, and so triangles naturally emerge [21,22]. Small group-level interactions continue up to create medium-sized meso-scale structure, producing modular clusters of nodes. These dynamic interactions are often collapsed into static contact networks for researchers where the above dynamics produce rich local structure at multiple size scales. It is tricky to precisely define multiscale local structure. Precise formulations of specific local network structures and statistics often operate at an implicit or explicit size-scale. For instance, clustering coefficients specifically target triads and can omit information related to higher-order structures. Other notions such as centrality, are global measures that can be insensitive to local information. Meanwhile empirical networks exhibit a rich multiscale structure [13, 23] with important implications for epidemic spreading [19,20]. When made precise, this implicit size-scale can produce unintended consequences when viewed at different scales (e.g., modularity resolution limit [24,25]). To mitigate this specificity issue, we

measure local structure in a multi-scale fashion using the network community profile (NCP) [13,26]. The NCP plot was introduced as the minimum conductance as a function of size-scale, in order to qualitatively study purely structural bottlenecks in a multi-scale fashion. The conductance of a set in a graph is a surface area to volume ratio, computed as the ratio of edges leaving a set (surface area) compared with the total edges incident on all vertices in the set (volume). The size-scale serves as a resolution parameter while conductance serves as the metric. Sets measured in the NCP differ from traditional community structure and related clustering measures because the sets are treated independently throughout the graph and hence, allowed to overlap. We adapt this structural measure for epidemics to create an *epidemic NCP* by using sets based on infection times for nodes over many epidemics. It may seem circular to define the NCP based on epidemic information rather than a purely structural network measure. However, using personalized PageRank as opposed to epidemic simulations yields qualitatively similar information and we include experiments comparing the two are included in Section E.4 in S1 Text. Fig 1 contains a detailed example for the computation of an epidemic NCP based on an SEIR epidemic model. These plots highlight multi-scale local structure in the wide dispersion of sets visited by epidemics, compared with random networks (Fig 1D vs. 1E).

Characterizing the impact of epidemic interventions

We quantify the impact of measured multi-scale structure by simulating epidemic spread while gradually removing this structure as we vary the amount of local quarantining. An example is shown in Fig 2 where we illustrate that multi-scale local structure causes local interventions to work far better compared to commonly used randomly rewired networks that lack such structure. Fig 2 displays the total fraction of infected nodes under various levels of local quarantining as we perturb the network to two extremes that lack any local structure. The first rewiring model (perturbation going to the left) rewires towards a random configuration model that preserves individual degrees in expectation. The second rewiring model (perturbation going to the right) rewires towards a uniform random network, preserving total edges in expectation. In both extremes, even high quarantine levels are unable to prevent large epidemic outbreaks. This should be contrasted with the original network which exhibits multi-scale local structure (the data illustrated here are from the Mexico City contact network [27]), where small local quarantine levels are able to quell large outbreaks. This illustrates that just because one reproduces a coarse summary statistic (e.g., average degree or degree distribution) does not mean that more subtle results such as response to epidemic intervention will lead to similar results as doing so in the corresponding empirical network (see Section F of S1 Text for an example of this with communities). In Section D.4 of S1 Text, we perform a separate study using a positive control where we use an approximate NCP rewiring procedure that preserves NCP information to a greater extent that other procedures. This separate study highlights some limitations of using the NCP as an assessment of local structure when the sets underlying the NCP have high correlations. This is particularly relevant for purely geometric structures. *Both studies highlight that interventions are very sensitive to the details of multi-scale local structure that are absent in popular baseline models.*

Central findings

Here is a summary of our main findings.

- We find that epidemics in empirically-measured interaction networks are much more controllable in terms of their response to a quarantine intervention, compared with widely-used synthetic network models of those same networks. We also observe larger dominant eigenvalues in the non-random networks — even though, based on popular baseline models, this would predict *stronger* and less controllable epidemics. (See Section 4.1.) These results suggest that characterizing multi-scale local structure is important to understanding epidemic spread in interaction networks, going well beyond simple summaries such as average degree or dominant eigenvalue.
- We provide a measure called Area Above the NCP (AANCP, see Equation 5) to quantify the amount of multi-scale local structure in a network. We find that this measure has a strong positive association with quarantine impact across a

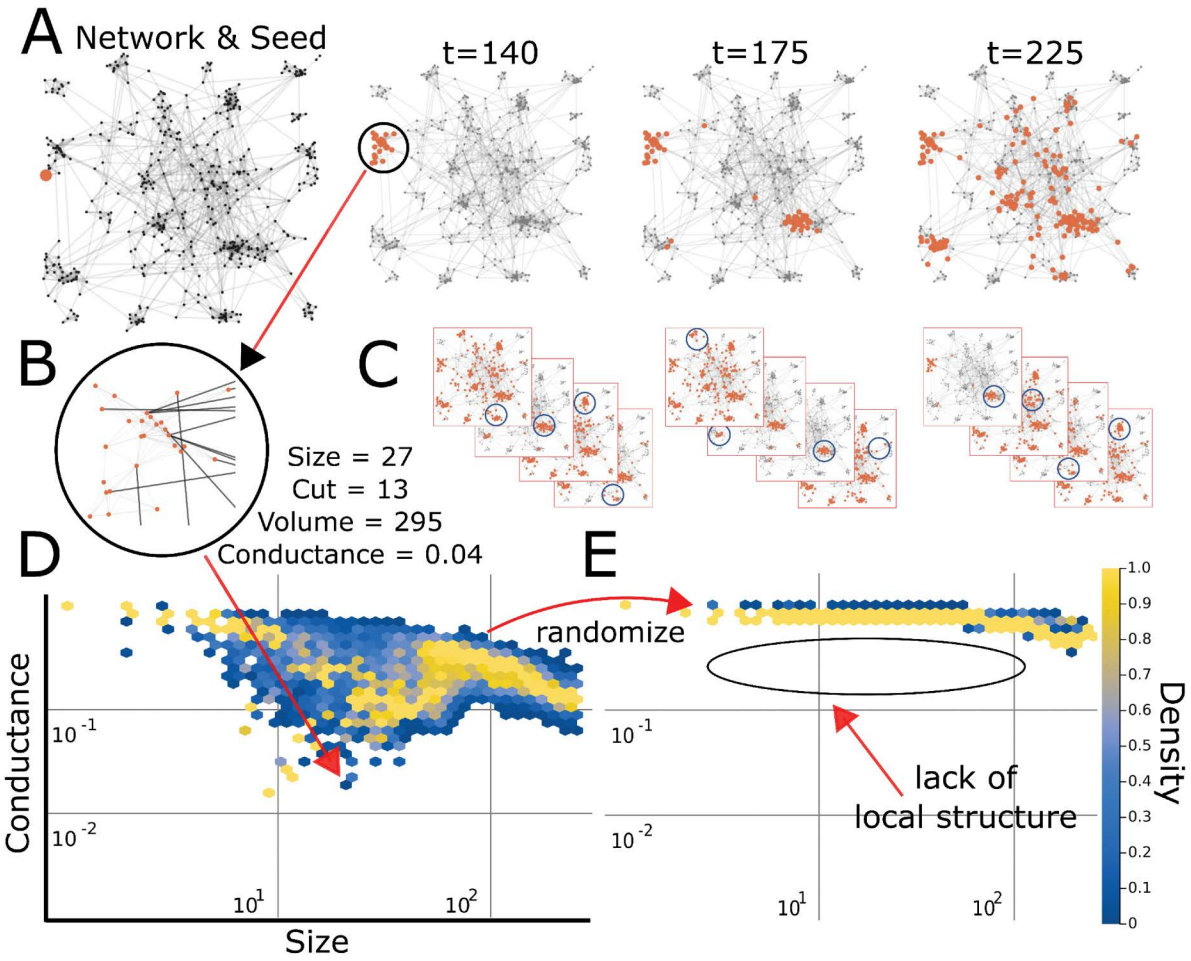

Fig 1. The Network Community Profile (NCP) characterizes local structure in networks by showing the distribution of local conductance bottlenecks at all size-scales. We use it to understand epidemic spreading by sampling conductance bottlenecks explored during epidemic spread. Epidemic NCP plots in (D) and (E) show a characteristic difference between networks with rich local structure (A and D) compared with a randomized network with the same degree distribution (E). (A) We initiate an SEIR epidemic from a given seed node and show a few steps of the spread where orange represents an infected or recovered node. (B) Sampling a single group of infected nodes at time $t = 140$ yields a conductance of 0.04 (cut to volume ratio is $13/295 = 0.04$). (C) This is repeated for tens of thousands trials over various seeds and sets. (D) Each sampled set yields a single point in the size-vs-conductance space, and the NCP is a distribution of these points. The NCP of the network in (A) shows wide variation in the size-vs-conductance space. (E) The epidemic NCP obtained by randomizing edges from the network in (A) with a configuration model. Minimal variability in conductance as the size-scale changes indicates a lack of local structure.

https://doi.org/10.1371/journal.pcsy.0000116.g001

variety of both real and synthetic models (Section 4.2). We cannot establish such a relationship for popular metrics, e.g., average degree or dominant eigenvalue.

- We further study the impact of multi-scale local structure in terms of understanding what sets are missed, i.e., not entirely infected, by the epidemic (Section 4.3). This highlights that low conductance sets are often protected from infection. This further supports the idea of associating a wide distribution of size-vs-conductance tradeoffs with this multi-scale local structure, because these missed sets occur at multiple size scales.
- We develop synthetic models to demonstrate how multi-scale local structure can emerge, as well as cleanly isolate its impact on epidemic spreading (Section 4.4). The first uses a geometry to produce local structure combined with plausible

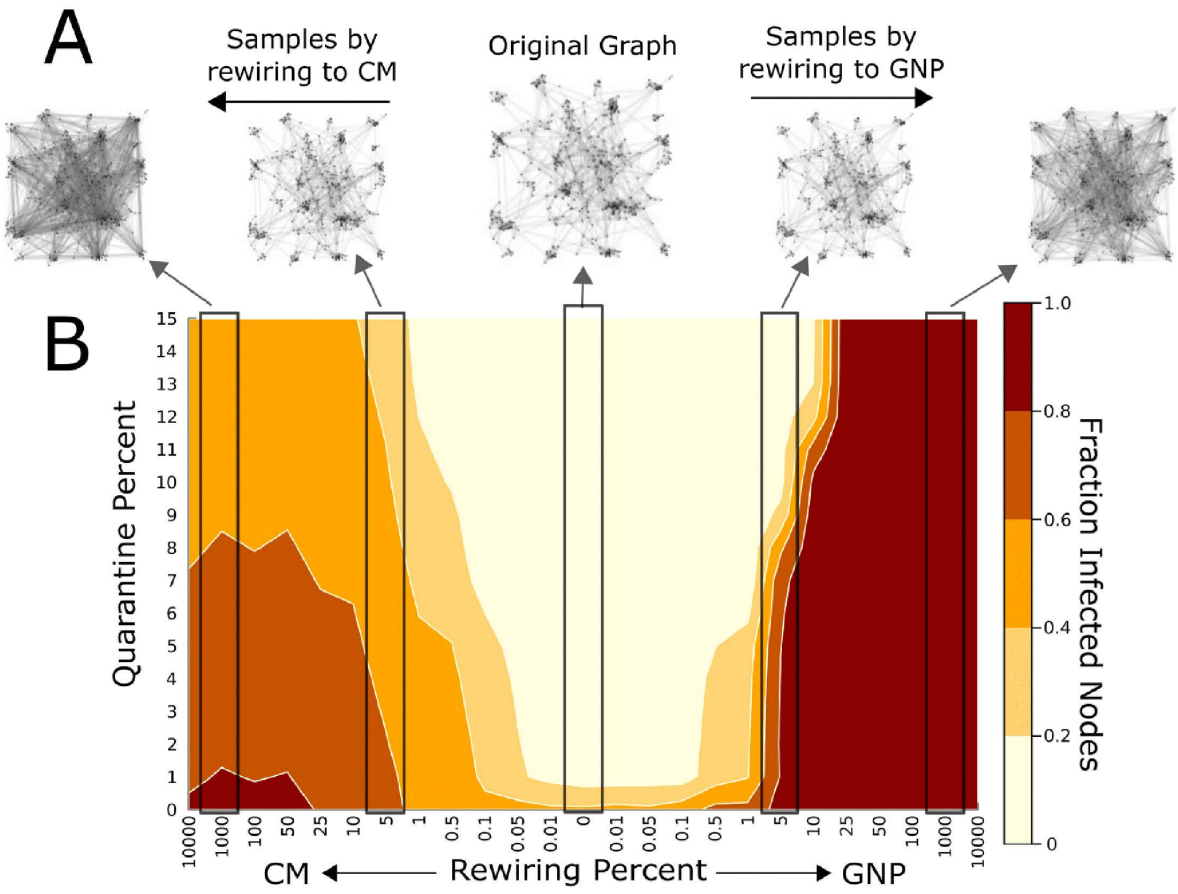

Fig 2. Networks containing realistic multi-scale local structure are more controllable under local interventions than networks lacking this structure due to prevalence of local bottlenecks. (A) Shows a network with local structure that is rewired to two different synthetic variants lacking local structure. For each rewired network sample, 800 SEIR simulations were performed - split among differing quarantine capacities. (B) Fraction of total infections as we tune both the maximum quarantine percentage (vertical axis) and rewiring percent (horizonal axis) for a mobility network based on contacts within Mexico City [27]. Note that darker represents a higher fraction of infections. All epidemics here use a fixed infection and recovery probability (0.02 and 0.05 respectively). Moving from center to left represents increasingly rewiring to a random configuration model (CM) that preserves node degrees in expectation; moving from center to right represents rewiring to a uniform random graph ($G_{n,p}$) that preserves average degree only. The network depicted in (A) is illustrative, as the Mexico City network does not admit a simple visual depiction.

https://doi.org/10.1371/journal.pcsy.0000116.g002

interaction and geometric preferential attachment models. The second (see Section B.3 of S1 Text) uses a random walk process as a surrogate for local geometry (recall that random walks diffuse slowly). These models illustrate compatibility between the rich multi-scale local structure and global quasi-randomness typically found in empirically measured networks.

- We conduct a separate study of epidemic spreading on hypergraph models to justify that the impact of local structure extends beyond simply using triangles as local structure (Section 4.5). This involves rewiring the triangles of a network.

2. Implications and relationships with existing literature

Surprisingly, this observation on the interaction of network structure, epidemics, and interventions has seemingly fallen between the cracks in disciplines that study epidemics and networks: *metapopulation models, network science, and computer science*.

Meta-population models seek macro-level simulation fidelity by using empirical mobility patterns among sub-populations [28–34]. These sub-populations are split based on spatial distance, and mobility data among regions is represented as a network of aggregated flow data [35]. Epidemic models are implemented on top of this mobility data taking into account characteristics of different regions as well as other patterns of human behavior, and they can include some level of heterogeneity [2,36]. Within a region and between regions, these models use mass-action or reaction-diffusion dynamics. This choice implicitly makes a local homogeneity assumption that differs from the types of local structure we observe empirically. These assumptions persist in various ways down into fine-grained event simulator models of epidemic spread, and they often result in overstating epidemic severity, e.g., erasing individual node identity [37] and related homogeneity assumptions [38]. A recent attempt has been made to address this overestimation [39] in total infections, but correctly calibrating parameters to match finer epidemic information remains a challenge. Such models are often used by epidemiologists, where the research goals are large-scale population level epidemic forecasts and intervention strategies for widely spread pathogens that are consistent with empirical data, rather than a detailed understanding of *what* properties of the network might give rise to these findings. We make use of static networks derived from human mobility data, not following the reaction-diffusion approach more common in meta-population models. Instead, we focus on structural bottlenecks that have implications for quarantining.

On the other hand, studies of the network structure itself (often by computer scientists or physicists) typically show that some structural network characteristic leads to qualitative differences in epidemic spread. This has been done in the mean-field or following other moment-closure based approaches [40,41]. Moment-closure approaches like mean-field approximations allow for idealized theory by reducing the complexity of the system of state update equations for node states [42]. Perhaps the most well-known of these approaches quantifies the epidemic threshold in the mean-field in terms of $\lambda_1(\boldsymbol{A})$ [40,41]. For the SIR and SEIR model, these approaches arrive at the following mean-field threshold for epidemics $s = \lambda_1(\boldsymbol{A})\frac{\beta}{\gamma}$. This in turn spurred follow up work that sought to mitigate epidemic spread by editing the graph a priori in order to minimize λ_1 and increase the parameter regime for which these for which epidemics vanish [43–45]. However, the dominant eigenvector $\boldsymbol{v}_1$ is known to be localized for empirical data [14,46], and this can distort the use of s to localized regions of the network. Other examples in the network science community range from heterogeneity in contact patterns [16–18] and community structure [47, 48] altering final epidemic size, to mixed impacts from multiple structural properties [49], to details of how the spatial network and interactions result in burstiness and possibly overcrowding treatment facilities [50]. Our findings highlight common scenarios where using this threshold to quantify epidemic strength and intervention effectiveness fails and networks with larger values of λ_1 have more effective interventions.

A separate line of research is concerned with designing interventions on networks via optimal control methods. These methods make use of networked data but don't *explicitly* probe the impact of that structure on spreading or interventions (see the survey by Nowzari et al., 2016 [51]). These are often formulated as a continuous-time Markov process and make use of tools from optimal control theory [32,34,52,53]. Two prominent formulations for epidemic interventions in the optimal control community are budget constrained and minimum-budget. In budget-constrained formulations, one minimizes $\lambda_1(\boldsymbol{B}-\boldsymbol{D})$ subject to cost constraints, where $\boldsymbol{B}$ is the matrix with node-to-node infection rates while $\boldsymbol{D}$ is the diagonal matrix of node recovery rates. In the minimum-budget formulation, the cost of interventions that decrease infection rates, $f_{i,j}(\beta_{i,j})$ or increase recovery rates $g_k(\gamma_k)$ are used to constrain solutions. These methods were global and apriori in nature. However, there are optimal control studies that seek to localize interventions at a node level [53,54] or perform interventions in an online rather than offline fashion [34,55,56]. While such formulations seek to constrain or contain spreading, neither probes what specific structures lead to more or less controllability.

Finally, our research is most closely related to the study of community structures and epidemic spreading. In particular, it was shown that networks with larger modularity [47] were found to have smaller total infections. This spurred follow-up work that attempted to mitigate epidemic spread by targeting nodes and edges based on community membership as well

as other structural factors in a local [57,58] and global [59–61] setting. However, there are many quantifications of what "community structure" entails. This results in ambiguity within the literature and mixed effects from community-targeted interventions [62,63], and it calls into question the impact of exact intra-community structures [64] in dense communities. Broadly, this ambiguity lies in both the size and mixing patterns of communities. For example, one study [65] showed that community mixing patterns in networks with identical values of modularity can significantly influence total infections and that this effect is amplified with more communities; while another study [48] showed that the infected fraction within communities is smaller in communities with less nodes.

Two prior studies have been conducted on multi-scale structure and epidemic spread. The first used a simplistic hierarchical meta-population model (containing nested multi-scale structure) to highlight heterogeneity in final epidemic size [19]. As we show in Section G of S1 Text, the multiscale nature created by this specific nesting type is different from the types of structure we find in empirical networks. The second utilized a metapopulation model coupled with a multiscale mobility network to find that long-range connection broadly determine the global behavior of epidemics [20]. We find something similar in terms of the epidemic spread when we construct synthetic models with local structure 4.4, but also how the long-range expander nature can be blunted via local structure and local interventions. In summary, while both studies use multiscale structure, neither studies interventions and they make local homogeneity assumptions implicit in meta-population methods that can impact epidemic spread in significant ways [37,38]. Our quantification of local structure as size-vs-conductance tradeoffs allows for analysis at all size regimes to resolve such ambiguities while using realistic networks. In particular, our multi-scale size-resolved approach is calibrated to avoid the ambiguity in community structure, and it shows that networks with modular portions at many size scales admit conductance bottlenecks that can be exploited to mitigate epidemics.

3. Methods

3.1 Data

Our findings are based on multiple empirically-measured networks that range in size from 10^3 nodes to over 10^6 nodes and that are plausible realistic substrates for epidemic behavior. Properties of these networks are summarized in Table C in S1 Text. These networks include a contact network for Mexico City [27], aggregated US commuting data [66], cellular mobility data [35], friendship networks from colleges [67], citation and collaboration networks [68–70], location based social networks [71,72], among others [13,73–77]. The networks were chosen to represent a diversity of possible realistic phenomenon and behaviors that go well beyond popular idealized models.

The raw data from these networks were processed to remove structural artifacts. In particular, small conductance sets at large size scales were removed (see Section C.1 of S1 Text for more information). As an example, in the college networks, the incoming class of freshman formed many connections among other freshman due to the timeframe when the networks were collected. This reflects a different process from students in other class years [78]. In order to more readily observe effects of local structure, the college friendship networks were further sparsified to highlight local heterogeneity. We used a simple method of sparsification where each node ranks its neighbors based on normalized common neighbors and elects to keep some fraction of edges based on that ranking. This is designed to model the most *likely* interactions to simulate the highest probability of epidemic spread. See Section C.2 in S1 Text for additional detail on this sparsification.

There are 15 static networks we study throughout in the main text:

Human Mobility

US Commutes, Mexico City, US Flows

Sparsified College Friendships

Illinois, Penn, Wisconsin

Electronic Social Interactions

Collaboration, Email, Facebook Interactions

Distant Networked Interactions

Citation, Slashdot, Flickr

Synthetic

Local Geometric, GeometricCommunities, RandomWalkCommunities

These networks are loosely ordered in terms of relevance to epidemic spreading, with the human mobility data most relevant, and the distant networked interactions least relevant. The synthetic network *Local Geometric* is meant to represent a purely local connections in a planar geometric (details in Section B.1 of S1 Text. In comparison, the synthetic networks *GeometricCommunities* and *RandomWalkCommunities* are meant to emulate more plausible combinations of local structure as well as large scale randomness. We discuss both of these further in Section 4.4.

3.2 Epidemic methods

We make use of the standard SIR and SEIR compartmental models with local quarantining. Nodes are partitioned by current infection state (state S – susceptible, state E – exposed, state I – infected, state R – recovered) along with an overlapping class Q for quarantining. Nodes in S that undergo quarantining (Q_S) are returned to S after the conclusion of quarantining. Nodes in E or I that are quarantined (Q_I) are moved to R at the end of the quarantine period.

Let $S^{(t)}$ denote the set of nodes that are susceptible at time t and likewise for $E^{(t)}$, $I^{(t)}$, and $R^{(t)}$.

Let $Z_v^{(t)} = Pr(v \text{ not infected at time } t) = \prod_{u \in N_v}(1 - \beta \chi_{u \in I^{(t)}})$ where β denotes the infection probability and $\chi_{u \in I^{(t)}}$ is an indicator function for node u being infectious at time t. A discrete time probabilistic formulation of the SEIR model can be given by

$$Pr(v \in S^{(t+1)}) = Pr(v \in S^{(t)}) Z_v^{(t)} \tag{1}$$

$$Pr(v \in E^{(t+1)}) = Pr(v \in E^{(t)})(1 - a) + Pr(v \in S^{(t)})(1 - Z_v^{(t)}) \tag{2}$$

$$Pr(v \in I^{(t+1)}) = (1 - \gamma) Pr(v \in I^{(t)}) + a Pr(v \in E^{(t)}) \tag{3}$$

$$Pr(v \in R^{(t+1)}) = Pr(v \in R^{(t)}) + \gamma Pr(v \in I^{(t)}) \tag{4}$$

In the above, a is geometric random variable that represents the probability a node in state E transitions to state I. This corresponds to the incubation period where a node is infected but not able to infect others. The variable γ denotes the probability of a node developing permanent immunity.

We use a local quarantining procedure where nodes can be quarantined via one of two mechanisms. Nodes can either be randomly selected or are the neighbor of a randomly quarantined node. We do not recurse on neighbors. A schematic figure is given in Fig 3. A more detailed description can be found in Section A of S1 Text.

Epidemic spread is simulated while varying contact structure, intervention strength, and infection probability. Each epidemic simulation occurs on a static network. Intervention strength and infection probability are purely epidemic parameters, while network structure is topological. For each parameter set, we start the epidemic from a single node. We repeat

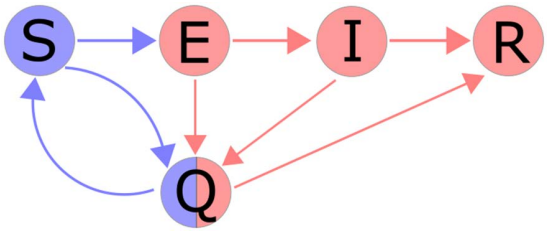

Fig 3. A schematic representation of transitions between disease states. S, E, I, and R form a partition of the nodes. A node can only transition out of Q into either S or R.

https://doi.org/10.1371/journal.pcsy.0000116.g003

this from 50 random nodes and record epidemic information including total infections and explored local structure for that set of parameters. Each simulation is run until the epidemic dies out. For each network, we also record the dominant eigenvalues of the adjacency matrix, which has been implicated in epidemic spread [40,41].

When selecting epidemic parameters, one often chooses parameters relative to the epidemic threshold [40,41], defined as $\frac{\beta}{\gamma}\lambda_1(\boldsymbol{A})$, where $\beta, \gamma, \lambda_1(\boldsymbol{A})$ respectively denote the infection probability, recovery probability, and dominant eigenvalue of the adjacency matrix $\boldsymbol{A}$. However, we want to make direct comparisons across synthetic variants of the same network. The dominant eigenvalues of these networks can differ dramatically – a point we return to in Section 4.1 (and see Fig 5) – which would change epidemic parameters. Since we want to simulate the spread of the same pathogen across rewired versions of the same graph, we often fix epidemic parameters (β, γ) when simulating spread on a network and its rewired variants (see Section A.2 of S1 Text for details). In instances where we compare one network to another network that differs in average degree (see Fig 9), we make these comparisons based on a fixed value of $\frac{\beta}{\gamma}\lambda_1(\boldsymbol{A})$.

3.3 Quarantine procedure

We use probabilistic discrete time SIR and SEIR models with quarantining. In a standard SEIR model, nodes are partitioned among the states susceptible - S, exposed - E, infectious - I, and recovered - R. A node can transition from one state to another depending on its own status and the status of its neighbors. A diagram of state transitions for the SEIR model with these quarantine transitions is shown in Fig 3.

Note that for the triangle rewiring experiments, we used a hypergraph diffusion which differs slightly, see Section A.3 in S1 Text). The recovery probability is fixed in all experiments to $\gamma = 0.05$ so that, on average, nodes are infected for 20 time steps. This choice is made to fix the time scale of the epidemic. We fix $a = 1/5$ so that, on average, nodes spend 5 time steps in the exposed class. All epidemics are initialized with a single infected node. All epidemic simulations were repeated from 50 random seeds. Where possible, we avoid averaging over separate epidemics and represent results via distributions.

We perform local quarantining by moving a node and its immediate neighbors to state Q. Note that this is similar to, but distinct from, acquaintance quarantining [79] since we quarantine all neighbors rather than a randomly selected neighbor.

We make several simplifying assumptions related to quarantining that aim to mitigate trivialities such as immediately halting the epidemic but still keep the quarantining policy local in nature. These assumptions are listed below:

1. Fixed quarantine period of $1/\gamma$ with no partial or early exit.
2. Fixed epidemic detectability threshold of 100 nodes.
3. Node detectability delay of 1 time step.
4. Neighbor quarantine delay of 1 time step.

5. A maximum quarantine capacity in the range of 0 – 15% of nodes.

Assumptions (2–4) are to mitigate against trivially halting the epidemic or quarantining too aggressively. Assumption (1) is a simplifying assumption for computational ease. More details on quarantining can be found in Section A.1 of S1 Text.

3.4 Network community profiles

The Network Community Profile (NCP) displays the distribution of size vs conductance for many sets of nodes in a network. Originally, the NCP was designed to highlight structural properties of social and information networks (in the minimum envelope of the samples for a conductance minimizing procedure). However, it has since been used to study the behavior of processes on networks more generally [26,80,81] and differs from classical notions such as k-core decompositions [82,83]. Consequently, there are many distributions of node subsets that can be defined. For the epidemic NCPs we use here, the sets are derived from epidemic spread itself. In particular, we sample 50,000 seed nodes; and, for each trial, we simulate epidemic spread for an SEIR model from each node 20 times. We combine the diffusions from each trial, and we use aggregated infection times for each node as a node ranking. Using this node ranking $\boldsymbol{s}$, we sequentially compute the conductance of the sequence of sets defined by the top ranked nodes. Explicitly, we are forming sets, S_k, consisting of the top-k ranked nodes and then finding their conductances. Note that the process of forming sets of top-k ranked nodes, S_k, and computing conductance values of this sequence is known as a sweepcut [84] in the local community detection literature. From there, we sub-sample several sets on a uniform-log scale using several bins in order to have size-vs-conductance information at all size scales. See Section E.1 in S1 Text for full details and modeling rationale on epidemic NCPs.

We also make use of another NCP based on personalized PageRank vectors. This PageRank NCP uses perseonalized PageRank vectors to form node rankings before computing conductance values via a sweepcut via the Andersen-Chung-Lang procedure [13,84]. In this instance, we can tune the locality directly via parameters from the underlying algorithm. In addition to storing information about sets, we explicitly store these sets. Storing the sets allows us to compare conductance minimizing NCPs with the epidemic NCPs. This allows us to display an NCP-like plot of the difference to highlight the nodes from the personalized PageRank NCP sets that were not infected during the epidemic. In this instance, each set from the personalized PageRank NCP is weighed based on the proportion of infected nodes from epidemic simulations. Thus each bin is weighed by the fraction of nodes in that bin that were in the S class at the end of several epidemic simulations without quarantining. Put simply, each bin reports the fraction of susceptible nodes in that bin. Values close to 1 indicate that nodes among sets in that bin were often avoided by the epidemic. Values close to 0 indicate most nodes among sets in that bin tended to become infected.

4. Main results

4.1 Empirical networks have worse epidemic thresholds but better interventions

Total infections often serves as a measure of the severity and strength of an epidemic. Recall that Fig 2 shows total infections as the fraction of infected nodes (color) as a function of intervention strength (vertical axis) and network structure (horizontal axis) for an SEIR model on a mobility network of Mexico City [27]. For the empirical network (the middle), relatively little intervention (quarantine) is needed to halt the epidemic. On the other hand, the randomly-rewired models, even with extensive quarantine levels, still result in a higher fraction of total infections. This results in a “U” shape in the plot.

The inability of random models without local structure to model epidemic behavior is not an artifact of this one network. Fig 4 shows similar effects for a large variety of networks (see Table C in S1 Text for properties of each network). These were deliberately chosen to span a wide range of different network types where the effects we describe are more or less pronounced. For instance, row (B) corresponds to sparsified college friendship networks, whereas row (E) corresponds to synthetic networks designed to emulate and possess local structure. The dramatic difference under quarantining observed

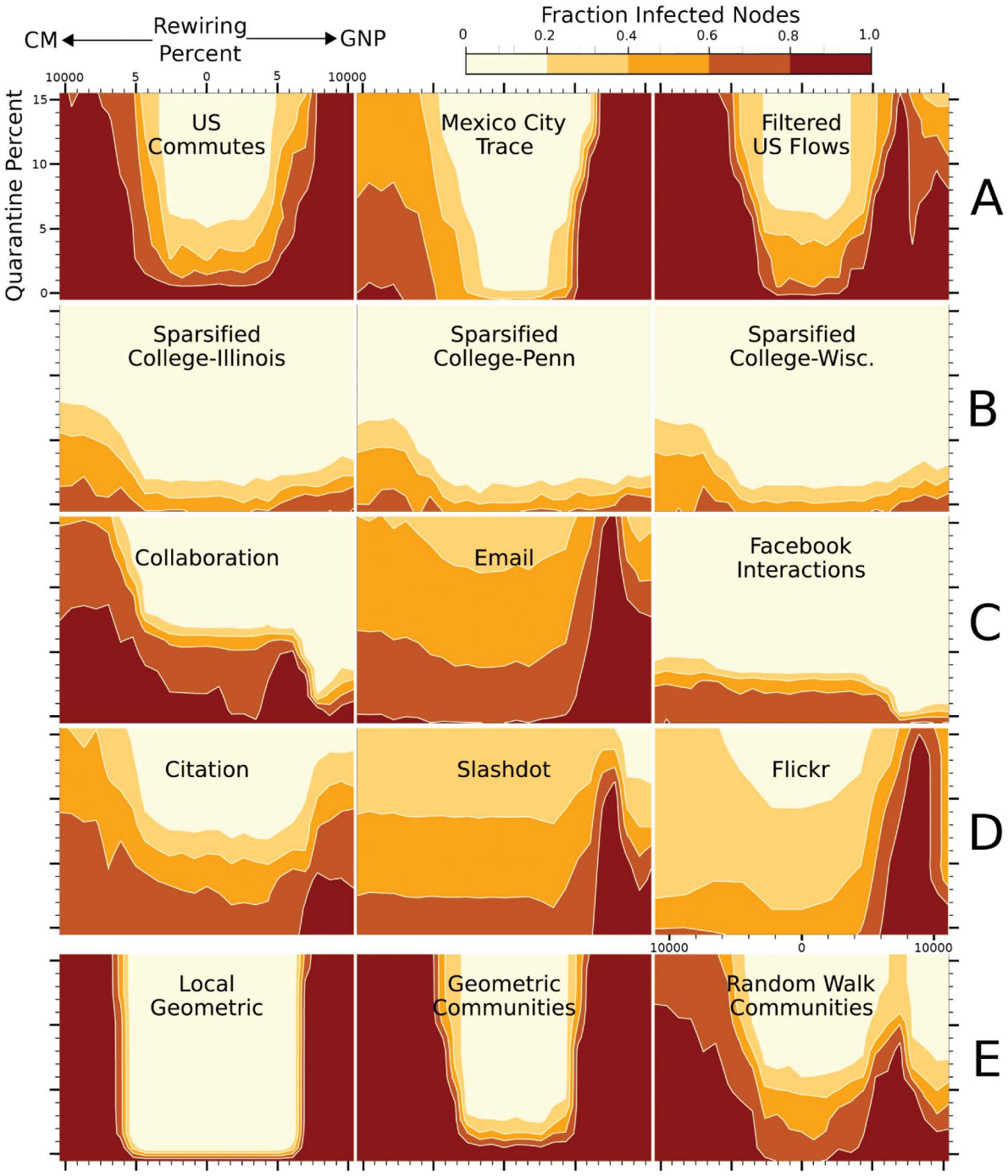

Fig 4. The presence of multi-scale local structure dramatically improves the impact of a quarantine intervention in an epidemic. Rows (A)-(E) show total infections as a function for rewiring (x-axis) and quarantine capacity (y-axis), as in Fig 2, for 15 networks. As we increasingly rewire networks (move away from the center), total infections deviates from those on empirical networks under local interventions. This effect is more pronounced in some networks (Row A) while absent in others (Facebook Interactions, etc). These results were produced using SEIR simulations on 50 node samples for each parameter set (quarantine percent and rewiring). See Section E.2 of S1 Text for details concerning choice of epidemic parameters.

https://doi.org/10.1371/journal.pcsy.0000116.g004

in Mexico City is present to differing degrees for many of the networks (US Commutes, Filtered US Flows, Citation, Flickr). On the other hand, networks where links have only a small basis in physical space display a range of effects (Collaboration, Email, Facebook Interactions, Slashdot). For two of the networks, Collaboration and Facebook Interactions, rewiring to $G_{n,p}$ produces a more controllable epidemic. Both of these have an extremely low average degree (6.3 and 3.5, respectively), which we believe is responsible for the difference in behavior. However, there is no straightforward relationship between the average degree and any of the effects beyond this. For example, all of the sparsified college networks have average degree around 3, and yet we see a different result there where rewiring to $G_{n,p}$ produces a stronger epidemic. Contrast this with S25 Fig, where an approximate NCP rewiring requires greater rewiring to see similar epidemic behavior.

Beyond average degree, epidemics in networks are often studied by their epidemic threshold: the critical value where the epidemic either explodes or dies off. This criticality threshold for epidemic spread under idealized conditions was shown to be proportional to the largest eigenvalue of the adjacency matrix, i.e., $\lambda_1(\boldsymbol{A})$, for various compartmental models [40,41] via mean-field approximations. The classical result is that the disease free state is asymptotically stable for an SIS model if $\frac{\beta}{\gamma}\lambda_1(\boldsymbol{A}) < 1$ and unstable when $\frac{\beta}{\gamma}\lambda_1(\boldsymbol{A}) > 1$. Hence, for these models, a larger value of $\lambda_1(\boldsymbol{A})$ indicates *stronger epidemic spread*. Moreover, the speed of extinction in the asymptotically stable case $\left(\frac{\beta}{\gamma}\lambda_1(\boldsymbol{A}) < 1\right)$ was shown to be exponential [40] ($Pr(v \text{ infected at time } t) \leq C\left(\lambda_1(\boldsymbol{A})\right)^t$). These results have spurred research into methods for mitigating disease spread by reducing the dominant eigenvalue either explicitly or via an approximation [43–45]. The main avenue of study is formulated as finding a subset of nodes/edges to remove from the graph so as to minimize the spectral radius of the resulting graph and reduce the parameter regime for which the disease free state is unstable. In other words, reducing the spectral radius increases the extinction regime.

To understand whether these theoretical results apply to realistic networks, we study values of $\lambda_1(A)$ as the networks are rewired in Fig 5. The original networks (red marker in subplots) all have larger values of λ_1. Contrary to what might be expected given the preceding discussion, λ_1 is *not* predictive of intervention effectiveness. Despite larger eigenvalues, many of the epidemics on the original networks are easier to disrupt and hence are more controllable. Referring back to Fig 4, most of the original networks exhibit fewer total infections compared to rewired variants, despite having larger spectral radius and hence a smaller extinction regime. Moreover, as networks are rewired, most eigenvalues decrease monotonically. Despite this, total infections can exhibit a spike when rewiring to GNP under quarantining (Email, Slashdot, Flickr, RandomWalkCommunities).

These results suggest that minimizing the spectral radius is not appropriate for empirical data containing multi-scale local structure. The idea behind minimizing spectral radius is to extend the extinction regime in the mean-field, under the assumption that this is a good heuristic for mitigating spread. However, this provides no information about epidemic indicators such as total infections, maximum infections, etc, when one is far from that threshold. Moreover, the spectral radius is fundamentally a global metric that can be locally distorted. One reason for this lies in the empirical localization of the dominant eigenvalue in empirical networks [14]. A previous line of work [14,46,85,86] has demonstrated the impacts of such localization on epidemic spreading for targeted intervention. By way of analogy, the spectral radius measures how easy a material is to ignite rather than measure how difficult it is to extinguish. Consequently, a large spectral radius indicates how easy it is to start an epidemic on the network rather than a forecast of an ongoing epidemic.

4.2 Local structure modulates epidemic spread under local intervention

The relationship between controllability and epidemic behavior can be understood through the degree to which local structure manifests in these networks. Intuitively, we expect that smaller conductance values at multiple size-scales should correspond to more successful epidemic interventions. This is due to local interventions being able to exploit near-by bottlenecks. Fig 6 shows the epidemic NCP for the same set of networks as in Fig 4. Recalling our analogy with local structure as high diversity of sets visited by epidemics, we note that networks where interventions are better able to curb spreading tend to have larger support in the size-vs-conductance space.

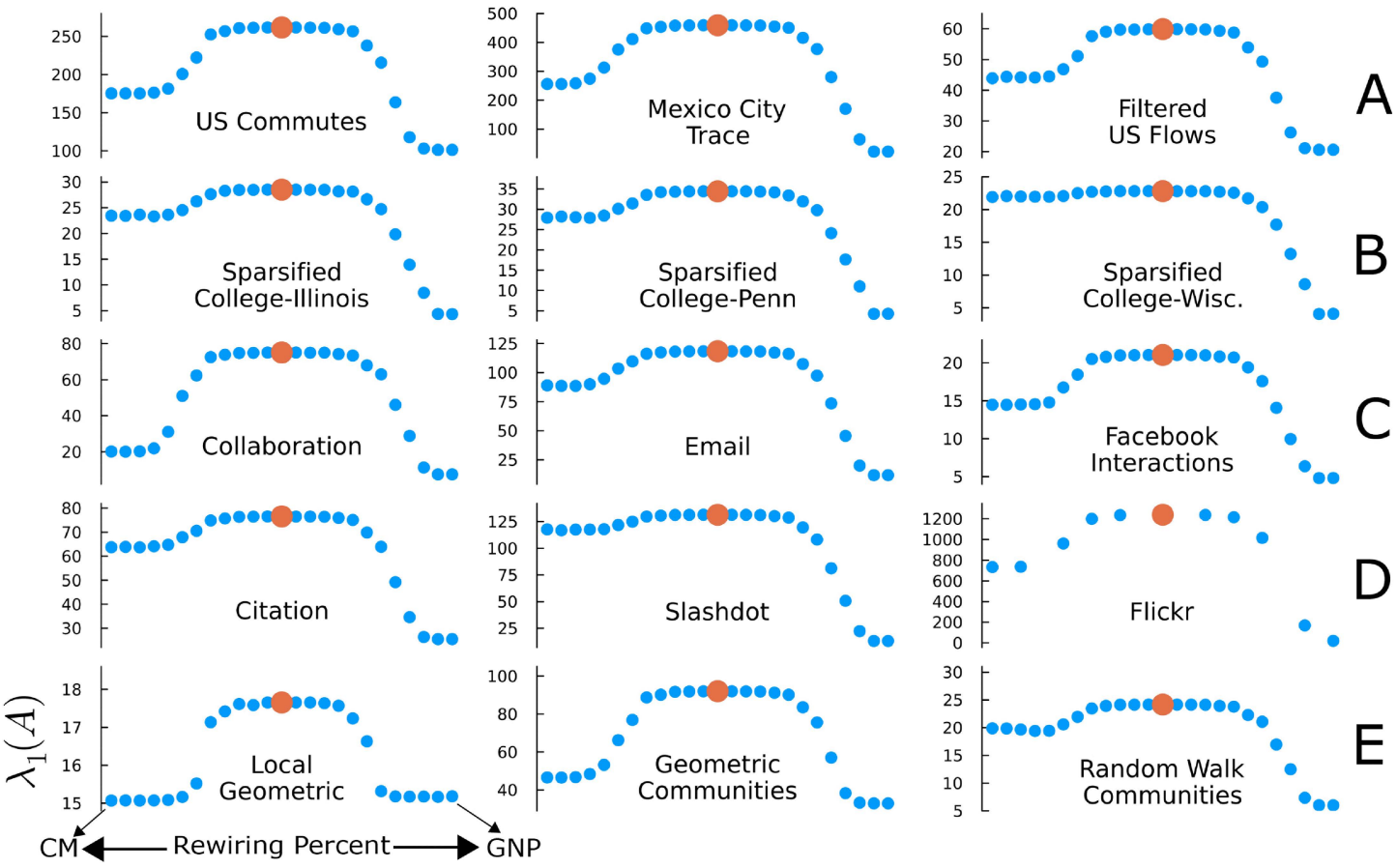

Fig 5. Using the epidemic threshold as a measure of epidemic strength would predict that higher values of λ_1 produce infections that are harder to control. However, the opposite result holds for these empirically measured networks. We display the dominant eigenvalue $\lambda_1(\boldsymbol{A})$ of the adjacency matrix ($\boldsymbol{A}$) vs the same CM ← Original → GNP rewiring on the horizontal axis (omitted for clarity). As we move from the center to the left (right) we are increasingly rewiring to CM (GNP). The original networks have larger eigenvalues, yet, comparing with Fig 4 shows that almost all of these epidemics require smaller interventions than synthetic variants to impede or halt spreading, contrary to what would be expected from eigenvalues alone.

https://doi.org/10.1371/journal.pcsy.0000116.g005

This led us to take an *area-based* measure of the support of the NCP plot as a quantitative measure of local structure at multiple size scales. The specific measure we compute is a normalized version of the Area Above the NCP (AANCP). If $\boldsymbol{x}$ is a normalized measure of set-size (maximum on x-axis in Fig 6 normalized to 1), and $\boldsymbol{y}$ are the minimum values from the NCP at the corresponding values of set-size, then we use

$$\text{AANCP}(\boldsymbol{x}, \boldsymbol{y}) = \text{AUC}(\log_{10}(\boldsymbol{x}),\ -\log_{10}(\boldsymbol{y})), \tag{5}$$

where AUC denotes the traditional Area Under the Curve metric. Equation 5 is simply the normalized area from maximum possible conductance $\phi = 1$ to the observed minimum in empirical sampling (further details in Section E.3 of S1 Text). This measure is closely related to the notion of the minimum envelop used in the initial literature on the NCP [13]. While the authors used the minimum conductance to define the NCP, we use normalized area above the minimum to capture the size of the support. Larger AANCP values correspond to a greater amount of multi-scale local structure. As an example, geometric networks should have large AANCP values while connected components of uniformly random graphs have smaller values. Compare the areas of panels D and E of Fig 1. While we use epidemic NCP which is motivated by

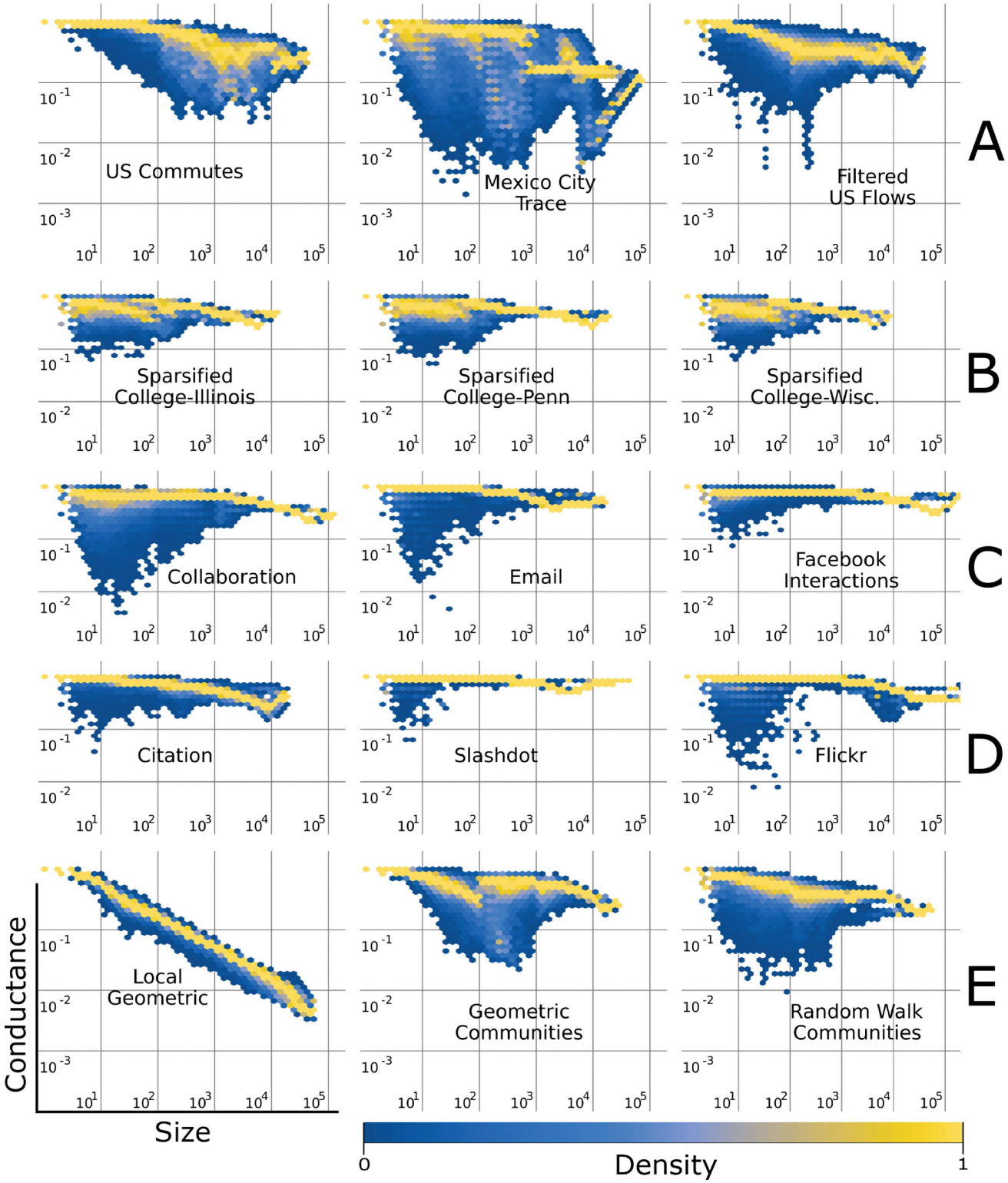

Fig 6. Local set structure explored by epidemics in these conductance-vs-size plots for graphs derived from the 15 networks. Mobility networks (row A) have some of the highest diversity in sets explored, whereas networked interactions (rows C and D) have lower diversity in this space. Compare with Fig 4.

https://doi.org/10.1371/journal.pcsy.0000116.g006

epidemics and uses dynamic information, one could also use purely structural information via personalized PageRank vectors to construct the NCP. Experiments comparing the two are included in Section E.4 of S1 Text.

Using Equation 5, Fig 7 shows that, as a measure of local structure, AANCP has a positive association with quarantine impact, while average degree and the dominant eigenvalue do not (middle and rightmost subplots). One would expect that average degree and dominant eigenvalue have a negative association. However, the presence of multi-scale local structure distorts this quite substantially. Fig 7 contains a network as well as its CM rewired variant, and it shows that the difference in quarantine impact in the presence of local structure can be quite substantial. Quarantine impact is quantified as

$$1 - \frac{\text{average infections under quarantining}}{\text{average infections without quarantining}}, \tag{6}$$

so that values close to 1 indicate that quarantining was very effective while values close to 0 indicate quarantining had no impact. (Additional statistics discussions on these results are given in Section E.3 of S1 Text.)

4.3 Local structure is indicative of who does not get infected

Multiple local [47,57,58] and global [59–61] immunization strategies have been proposed for networked epidemics that explicitly target nodes or edges based on the modular structure of networks. Implicitly, these methods seek to contain epidemic spread by making the networks more modular by targeting nodes and edges that accelerate spreading (e.g., community bridges or hubs). Fig 6 suggests that epidemic spread is global since for most networks, higher conductance sets are explored far more often than low conductance sets at all size scales. Moreover, lower conductance tends be seen at smaller sized sets. What this suggests is that very good conductance sets (i.e., communities) may be more indicative of what portions of the graph are *not* explored. To support this point, we explore the extent to which an epidemic fails to infect extremal conductance sets.

Fig 8 shows that sets at small sizes with smaller conductance values resist infection and serve as barriers to infection (Columns 3–6). Columns 3–6 show the evolution of node susceptibility in the size-vs-conductance space. As the infection strength (β) increases, the portion of these NCPs more likely to remain susceptible are sets that have low conductance and small size (bottom left of individual plots in columns 3–6 of Fig 8). Overcoming these conductance bottlenecks

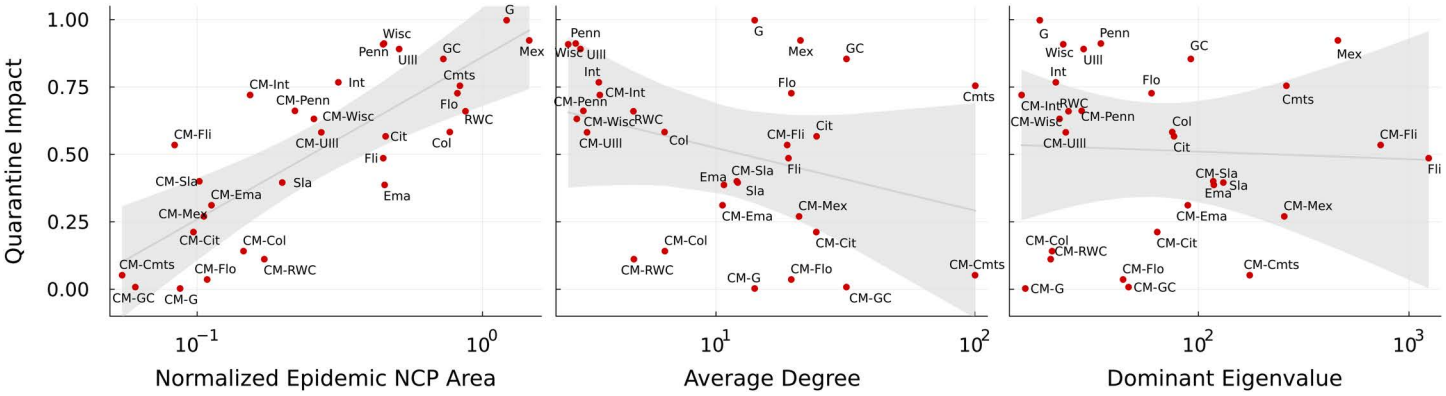

Fig 7. Local structure has a positive association with effectiveness of local interventions while measures such as $\lambda_1(A)$ and average degree have little or no correlation. When we use normalized area above NCP, AANCP (see Equation 5), of the epidemic NCP as a measure of local structure (horizontal axis in leftmost plot) and quantify the impact of quarantine as in Equation 6, we then find a positive correlation (Spearman ρ correlation coefficient 0.78 with 95% CI [0.58,0.89] using $n = 30$ graphs). Values close to 1 (the maximum impact) indicate that quarantining was more effective. Epidemic parameters used for the data shown are the same as those in Fig 4.

https://doi.org/10.1371/journal.pcsy.0000116.g007

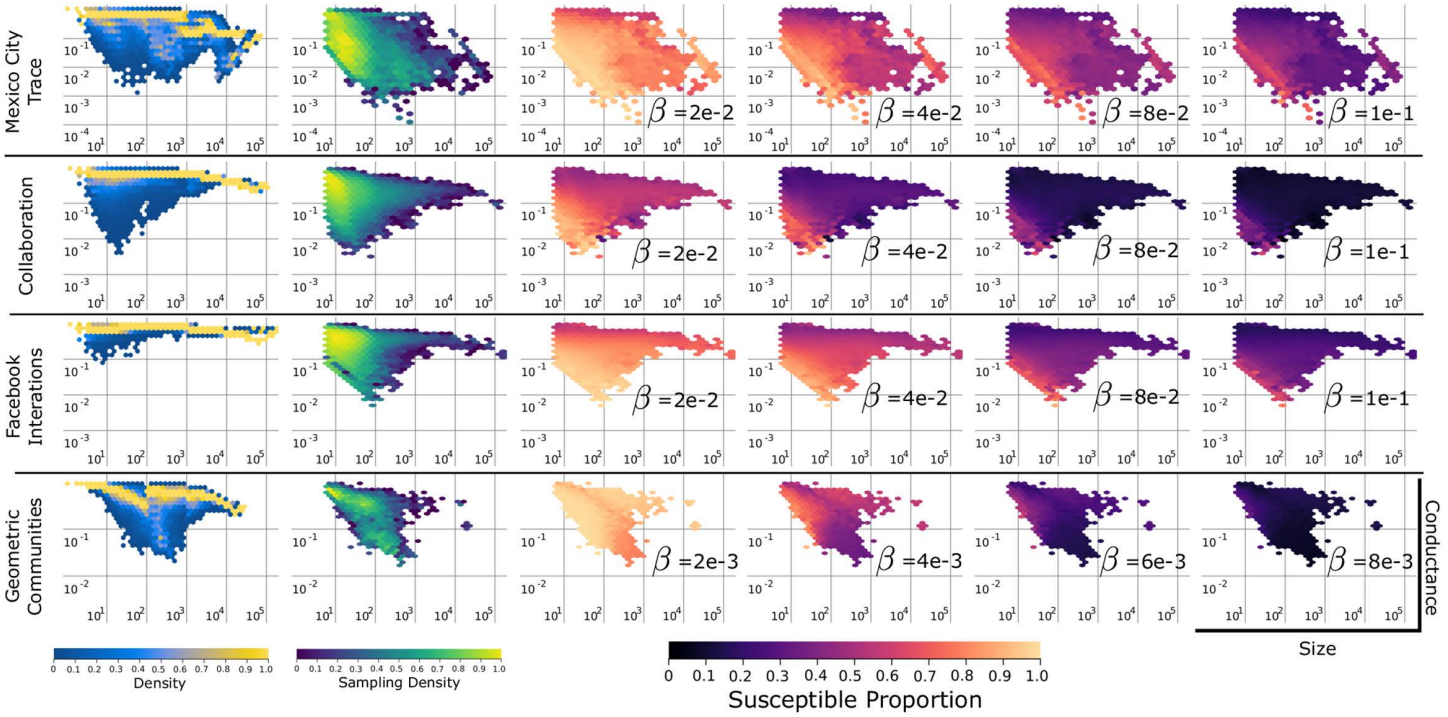

Fig 8. Small conductance sets at small sizes serve as barriers to infection. The first column shows the epidemic NCP. The second column uses personalized PageRank vectors to better sample extremal conductance sets at small size scales. Columns 3-6 uses sets found by personalized PageRank vectors but weighs each set according to the proportion of nodes susceptible at the end of 50 SEIR epidemics. Nodes in low conductance sets at small size scales are more resistant to infection and require larger infection probabilities (β) for epidemics to reach those nodes. This suggests that these sets serve as local mixing bottlenecks and provide barriers to infection. Epidemics in this figure do not use any quarantining. The recovery probability is fixed at γ = 0.05 while the infection probability, β, is displayed in columns 3-6.

https://doi.org/10.1371/journal.pcsy.0000116.g008

requires even stronger epidemics. Sets in columns 3–6 are derived from a different NCP that uses personalized PageRank information to retrieve sets with good conductance scores. This approach comes with strong theoretical guarantees [84,87] (see Section E.1 in S1 Text for more details). The local structure derived from personalized PageRank is combined with epidemic information to show susceptible nodes in the size-vs-conductance. While the epidemic NCP in column 1 gives us information about where the epidemic explored, the personalized PageRank NCP is used to better sample extremal sets at the small size regime. Put simply, the epidemic NCP is biased towards disease spread, while the personalized PageRank NCP is biased towards minimal conductance sets.

While previous research has noted lower epidemic prevalence in smaller sized communities [48,88], Fig 8 offers an explanation for *why* this is the case. These sets are harder to get into during epidemic spreading due to the nearby local mixing bottlenecks in the network.

4.4 Generative models of local structure

Empirical results from the realistic networks we have analyzed suggests that multi-scale local structure critically impacts the evolution of epidemics under localized interventions. However, realistic empirical networks are often a confounding mixture of many phenomena. We want to cleanly disentangle the impact of multi-scale local structure from other structural artifacts that may exist in empirical networks. To this end, we produce two synthetic models that generate multi-scale local structure in distinct ways. The first (GeometricCommunites) uses local geometry to add community structure while maintaining large scale

randomness. The second (RandomWalkCommunities) starts with planted community structure and adds local structure via local random walks, akin to what was studied in ref. [13]. We mainly discuss GeometricCommunities in the main text while leaving RandomWalkCommunities in Section B.3 of S1 Text. We discuss both as we wish to illustrate that the produced local structure is more important than the particular generating process that gave rise to that structure. Both models feature long-range edges or weak ties, the presence of which is know to impact disease spreading [89,90]. In both models, the impact of our local quarantine interventions are similar to the most realistic empirical networks formed from human mobility traces.

4.4.1 GeometricCommunities. The GeometricCommunities model seeks to create local pockets of community structure with large scale randomness. It also aims to produce networks that have a core-periphery structure [91] consisting of a large dense "core" and a "periphery" consisting of relatively small dense pockets that are loosely connected to the core. This feature of networks has been observed in a wide range of empirical networks [13,82,83]. We begin by assigning each node a random coordinate in a toroidal space (2d box with wrap around). Each node picks a degree from a log normal distribution and connects up to the nearest local neighbors. Each node also samples a much smaller number of neighbors randomly across the network to simulate weak global ties. Distances are computed in toroidal space (allowing wrap-around), while weak ties are selected in a preferential attachment manner, with high degree nodes adding more edges than low degree nodes. Node degree is then used as a proxy for node importance. Nodes *update* their positions by moving to their most important (highest degree) neighbor as a means to emulate social influence or homophily. Local edges are reformed while some fraction of weak-ties is maintained (details in Section B.1 of S1 Text). After updating positions and keeping weak ties, they reconnect to nearest neighbors to roughly maintain their degree. Each step of updating the node positions and reallocating links is called an iteration. Nodes that become disconnected are randomly re-initialized to simulate migration. We see the development of similar local structure (as measured by the NCP plots) in about 50–150 iterations. The goal is to induce community structure (local accretion to the high degree nodes) with large-scale randomness (weak ties) while maintaining some of the planted 2d geometry (coordinates). Note that the average degree in the network grows via this process because the connection decisions are made from either side.

4.4.2 Epidemic simulation results for generative models of local structure. GeometricCommunities is a generative model that produces rich multi-scale local structure while qualitatively matching observed epidemic behavior of empirical networks. Local interventions on GeometricCommunities can produce the same type of epidemic response on human mobility networks. This can be seen in Fig 4 by comparing row (A) to the subplot for GeometricCommunities (middle of row (E)). Moreover, the network produced by GeometricCommunities has qualitatively similar levels of multi-scale local structure as empirical mobility networks as depicted in Fig 6. This is further exemplified by Fig 7, as we compare epidemic response vs λ_1 and average degree. As a generative model with both geometry and long-range edges, we are further able to probe the impact of long-range edges on local structure and spreading. Long-range edges or weak-ties [90] are known to accelerate epidemic spreading [20,89,92] as well as to seed new local epidemics [93]. From this alone, we should expect that long-range edges should mask local structure. Fig 9 shows that is exactly what happens when one adds in long-range edges. As we move left to right column-wise, the networks on the right are derived from networks on the left by adding long-range edges (middle subplot) and then applying an iterative local homophily or social influence update to node positions and reforming local edges while preserving long-range edges. In doing so, the long-range edges completely masks the latent geometry in the network, while simultaneously accelerating spreading and reducing controllability. However, after 150 steps of the iterative node and edge update procedure, we arrive at the final network for GeometricCommunities which behaves like a spatial model (Local Geometric) with regards to local interventions but which has a wider distribution of local structure than a purely geometric network.

4.5 Triangle weighted diffusions

It is common to assume that local structure in networks is rooted in triangles and local clustering coefficients [22]. There are also relationships between regions dense in triangles and the network community profile [80]. To test this hypothesis

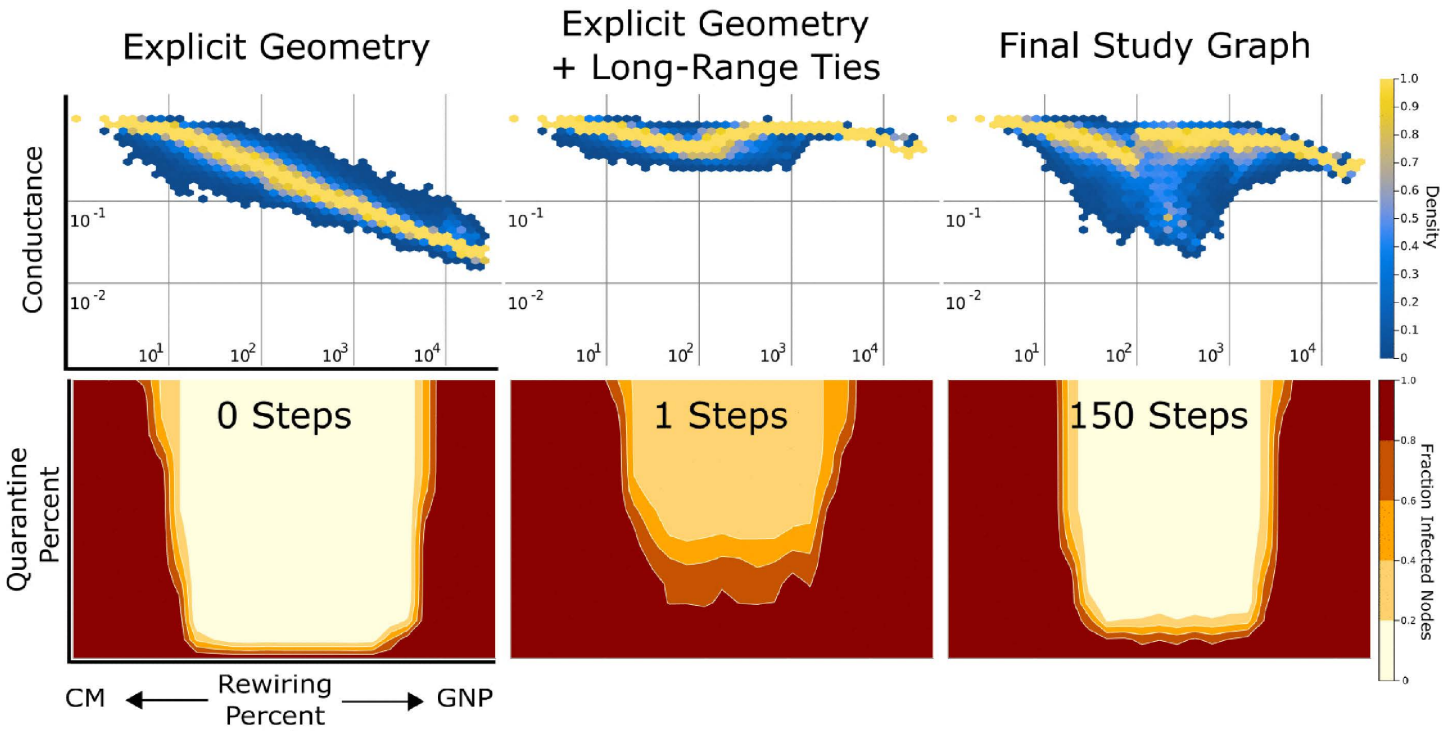

Fig 9. The GeometricCommunities model helps us understand how long-range edges can simultaneously mask multi-scale structure and reduce epidemic controllability. The first column shows the epidemic NCP (top) and total infections (color in bottom plot) for a network where edges are derived from explicit geometry. Minimal quarantining is needed to halt the epidemic entirely. The middle column shows the same information using the network in column 1 but adding a small fraction of long-range ties. This destroys local structure and dramatically reduces epidemic controllability, as larger interventions are required to mitigate spreading. The last column shows the same information for the network in column 2 after 150 iterations of the GeometricCommunities model in which we have both more local structure and the epidemic is more controllable. Epidemic parameters are chosen based on the epidemic threshold $s = \lambda_1(\boldsymbol{A})\frac{\beta}{\gamma}$ due to large differences in average degree (see Section E.7 in S1 Text for details).

https://doi.org/10.1371/journal.pcsy.0000116.g009

and determine whether our findings are simply a matter of the number of triangles in a network, we randomized the triangles of the network. One challenge with this experiment is that randomizing triangles produces changes to the number of edges, which makes it difficult to use the same epidemic parameters, as they are sensitive to average degree. To account for this effect, we simulate an epidemic on the hypergraph formed via triangles and edges.

4.6 Hypergraph weighted diffusions

We consider a hypergraph model of epidemic spread using triangles or edges as modes of disease spread. Each hyperedge represents a joint meeting of all nodes in that hyperedge. In particular, we allow triangles to serve as modes for disease transmission with the same edge infection probability, β. We also include pairwise-edges since otherwise spreading would be impossible on the triangle-free portion of the network. Fixing β for all edges and hyperedges allows this hypergraph model of spread to be expressed as a weighted pairwise model on the original network. (See Section A.3 in S1 Text for details and exact formulation.) Edges in the original graph, $\boldsymbol{A} = (a_{i,j})$, are weighted so that $w_{i,j} = \max(a_{i,j}, T_{i,j})$, where $T_{i,j}$ is the number of triangles in which nodes i and j jointly participate. The probability of infection along each edge is then given as $\beta w_{i,j}$. This hypergraph model is used on networks in which triangles are shuffled around the network so that the average driving force of the infection ($\sum_{i,j} \beta w_{i,j}$) is preserved as triangles move.

4.6.1 The impact of randomizing triangles. To randomize the triangles of the network, we treat each triangle as a hyperedge, and we randomize its endpoints at each step for up to a million steps. Fig 10 shows that for a majority of networks, triangles are insufficient to model local structure under the above hypergraph weighted diffusion using the same quarantine intervention as in the pairwise case. The leftmost side of each subplot represents the original network. As we move to the right, the triangles in the network are increasingly shuffled. There are three distinct types of observed phenomena (demonstrated by the rightmost subplots of rows A, B, E). Case 1 (triangles insufficient) is exemplified by Filtered US Flows, Case 2 (triangles sufficient) by Sparsified College-Wisc, and Case 3 (sensitive to parameters) by RandomWalkCommunities).

For most networks, *triangles are insufficient to model local structure*. This is Case 1, where shuffling of triangles requires more quarantining to stop spreading (e.g., row A). For a smaller minority of networks (row B and Facebook Interactions), triangles are the full extent of local structure. For the networks in row B, this makes sense since those networks were sparsified in a biased manner towards edges that participate in many triangles. Put simply: we sparsified them such that triangles are the only remaining local structure. Facebook Interactions (rightmost of row C) also exhibits the same behavior, even without this sparsification. Case 3 only occurs for RandomWalkCommunities (rightmost plot of row E). Here, triangle shuffling initially causes a large spike in total infections before dramatically reducing and becoming independent of total infections. If we ignore the initial spike, then we see behavior similar to case A in that the networks are harder to control after randomization.

5. Discussion

Our results highlight the significance of multi-scale local structure on epidemic spread and the effect of interventions on realistic network epidemics. We now discuss two related aspects: existing measures of epidemic strength; and community structure.

The reproduction number R_0 is canonically used to characterize the strength or severity of an epidemic [94]. The value of R_0 gives the expected number of infections that an individual will cause in a completely susceptible population. In the case of non-networked epidemics (epidemic modeling without access to network structure), the critical threshold for epidemic spread is $R_0 = 1$. However, in the SIR and SEIR networked case [41], $s = \lambda_1(\boldsymbol{A})\frac{\beta}{\gamma} = 1$ is the critical threshold in the mean-field. Despite this similarity between R_0 and s, we did not find a good use for s in terms of quantifying epidemics on realistic interaction networks. For example, in Fig 7, two networks can have similar values of λ_1 and s despite very different behaviors in epidemic spreading. Moreover, s is distinct from R_0 since R_0 is bounded above by average degree in a network while λ_1 is bounded in terms of the maximum degree of a network. The idealization of R_0 as the average number of secondary infections from a single primary infection is problematic in finite-size networks. We attempted to investigate this empirically and found little reliability in R_0 values as the epidemic progresses, hence we focus on the mean field approximation that would show R_0 is bounded by average degree. For some discussion of these issues and a few possible solutions that involve subtle changes to the definition of R_0, see [95]. The dependence of s on $\lambda_1(\boldsymbol{A})$ has further epidemic consequences due to known issues of localization in the corresponding dominant eigenvector [86,96]. Our results suggest that s should be interpreted as a best-case threshold in stochastic simulations, rather than a proxy of epidemic strength [43–45].

As previously mentioned, it is recognized that community structures are correlated with fewer infections [47] and have several local [47,57,58] and global [59–61] strategies for targeted interventions. However, the use of a metric like modularity can mask heterogeneity in community sizes and mixing patterns. The variability arises from the diverse nature of what constitutes "community structure." Moreover, community mixing patterns [65] as well as sizes [48] can alter the fraction of infected nodes within communities. For instance, a network composed of many small communities but smaller modularity can require smaller interventions than those composed entirely of medium or large sized communities but with larger modularity (see Section F in S1 Text for an example of this). The use of the epidemic NCP that we introduce examines all size-scales to overcome this

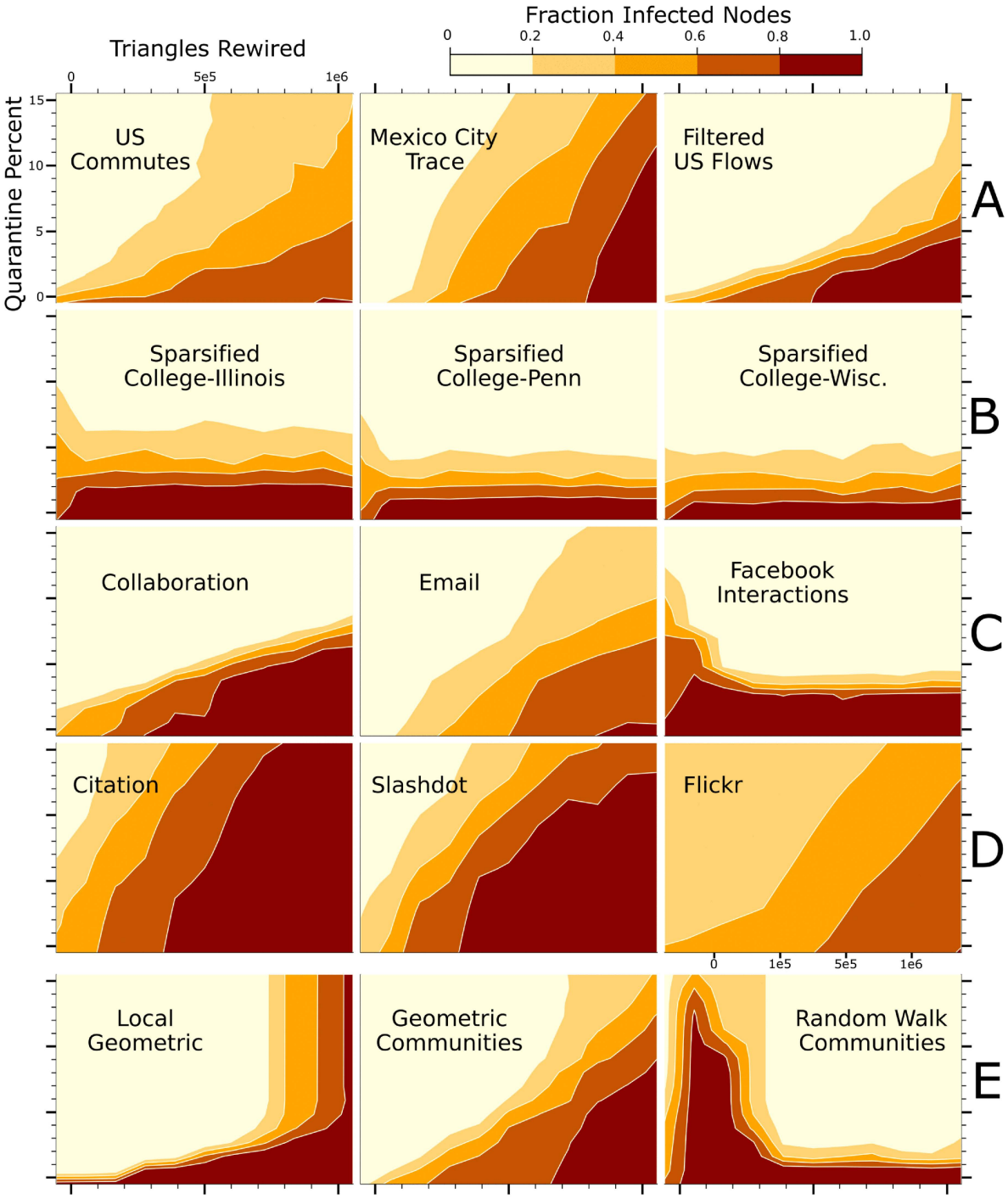

Fig 10. Triangles are insufficient to explain the effects of local interventions. To test this, we shuffle the location of triangles in the network (horizontal axis) and measure the impact of quarantine interventions (this is similar to one half of Fig 2). For most networks, randomizing triangles requires more quarantining to mitigate spread (Rows A and D, most of C and E). This shows that the local structure we study exists beyond local triangle structure because epidemic response varies as we shuffle triangles. See Sections E.2 and E.8 in S1 Text for details concerning choice of epidemic parameters.

https://doi.org/10.1371/journal.pcsy.0000116.g010

ambiguity. Furthermore, the epidemic NCP augments purely structural information on communities with epidemic spreading preferences (section 4.2). When combined with purely structural bottlenecks, we find that nodes contained in sets with small conductance and small size are harder to infect; and, in those cases, conductance bottlenecks serve as barriers to infection.

The modeling results show that local structure—in particular multi-scale local structure—can critically impact epidemic spreading. Practical success at mitigating epidemics depends on the relevance of the modeling regime in terms of speed with which interventions can be implemented. For instance, the speed of viral spread must be slow enough that interventions can meaningfully impact spread. Thus, our findings reiterate the importance and likely effect of targeted interventions: paid sick leave and rapid tests to effectively implement quarantine procedures along with contact reduction. Indeed, our results suggest that sparsifying a network in such a manner will, in general, reduce the speed of viral spread and enhance the role that local bottlenecks play in the network. This shows how multiple interventions may amplify the effects of each other in empirical networks. In contrast, synthetic models lacking multi-scale local structure often misrepresent how much intervention is required to impact epidemic spreading, let alone halt it entirely. This is due to the lack of local conductance bottlenecks in synthetic networks that do not reflect the realistic heterogeneity in human mobility data. This disconnect between common synthetic models and empirical data highlights the need for widespread access to human mobility data and synthetic models that contain realistic multi-scale local structure. The widespread access of models with local structure and human mobility data will enable policy choices grounded in real-world behavior.

There is also the question of implementations of interventions. Alternative interventions could have been performed and their impact on epidemics can be quite substantial [97]. In other epidemic contexts, e.g., spread among livestock, alternate intervention strategies may also be effective in mitigating spread [98]. While we performed extensive experiments over a number of parameters ($\approx$ 380,000 for each graph in Table C of S1 Text), we assumed 100% adherence to quarantining. This is an idealized case and speaks to the need for a real-time network for epidemic surveillance and disseminating information about positive tests. As was made apparent during the COVID-19 pandemic, not everyone will adhere to these interventions. A critical aspect to study in this regard is that intervention adherence may itself be network mediated phenomenon (e.g., through information and misinformation spread through both in-person and online social networks), which makes studying and modeling this aspect particularly challenging. This limits the generalization of our results to real epidemics as quarantine compliance, detection, and government interventions are far from idealized. Additional studies with network mediated quarantine compliance, limited detectability, and slower, uneven government interventions would help shed light on how realistic human epidemics would respond to more realistic interventions.

Finally, in terms of the prospect of future pandemics, our results here also reiterate the critical importance of monitoring, surveillance and early action in such regions prone to viral spillover [99], due to the increased potency of early intervention in networks of human mobility with local structure. For instance, it is estimated that over 60,000 people are infected with bat-based coronaviruses annually in southeast Asia [100]. That pandemics are not common may be related to the protective nature of multi-scale local structure in our contact networks.

Supporting information

S1 Text. Supplemental information text.
(PDF)

S1 Fig. US Commutes diffusion data. Epidemic "strength" (original network with no quarantining) varies from $s \approx 5$ to $s \approx 471$.
(TIF)

S2 Fig. Mexico City Trace diffusion data. Epidemic "strength" (original network with no quarantining) varies from $s \approx 18$ to $s \approx 919$.
(TIF)

S3 Fig. US Flows diffusion data. Epidemic "strength" (original network with no quarantining) varies from $s \approx 2$ to $s \approx 120$.
(TIF)

S4 Fig. Sparsified College-Illinois diffusion data. Epidemic "strength" (original network with no quarantining) varies from $s \approx 11$ to $s \approx 108$.
(TIF)

S5 Fig. Sparsified College-Penn diffusion data. Epidemic "strength" (original network with no quarantining) varies from $s \approx 14$ to $s \approx 131$.
(TIF)

S6 Fig. Sparsified College-Wisc diffusion data. Epidemic "strength" (original network with no quarantining) varies from $s \approx 9$ to $s \approx 87$.
(TIF)

S7 Fig. Collaboration diffusion data. Epidemic "strength" (original network with no quarantining) varies from $s \approx 3$ to $s \approx 150$.
(TIF)

S8 Fig. Email diffusion data. Epidemic "strength" (original network with no quarantining) varies from $s \approx 5$ to $s \approx 237$.
(TIF)

S9 Fig. Facebook Interactions diffusion data. Epidemic "strength" (original network with no quarantining) varies from $s \approx 4$ to $s \approx 76$.
(TIF)

S10 Fig. Citation diffusion data. Epidemic "strength" (original network with no quarantining) varies from $s \approx 2$ to $s \approx 138$.
(TIF)

S11 Fig. Slashdot diffusion data. Epidemic "strength" (original network with no quarantining) varies from $s \approx 5$ to $s \approx 263$.
(TIF)

S12 Fig. Flickr diffusion data. Epidemic "strength" (original network with no quarantining) varies from $s \approx 50$ to $s \approx 2481$.
(TIF)

S13 Fig. Local Geometric diffusion data. Epidemic "strength" (original network with no quarantining) varies from $s \approx 1$ to $s \approx 35$.
(TIF)

S14 Fig. GeometricCommunities diffusion data. Epidemic "strength" (original network with no quarantining) varies from $s \approx 2$ to $s \approx 184$.
(TIF)

S15 Fig RandowWalkCommunities. Epidemic "strength" (original network with no quarantining) varies from $s \approx 4$ to $s \approx 242$.
(TIF)

S16 Fig. (Best viewed in color.) Example of rescheduling disease transmission time after quarantining an infected node. At time t, u is scheduled to infect w at time $t+3$. This is the minimum infection time for w. However, when u is

quarantined at time $t+1$, we must figure out if the infection time for node w changes. In this example, it does. Node v infects w at $t+5$, and this becomes the new infection time for w.
(TIF)

S17 Fig. (Best viewed in color.) An example illustrating a rescheduling of infection times due to quarantining. Node w is quarantined at time $t=8$ but is susceptible after exiting quarantining. If either of u or v are infectious after w leaves quarantine, they may potentially infect w.
(TIF)

S18 Fig. The RandomWalkCommunities model emulates local structure by combining a very sparse LFR graph to plant community structure along with local structure that arises by adding edges with local random walks. This model exhibits qualitatively similar effects as Filtered US Flows under local interventions (see Fig 4). RandomWalk-Communities is generated with planted community structure augmented by local random walks. As the number of random walks increase (number of steps in figure increase), the model exhibits increasing levels of local structure (larger values of AANCP). Moreover, epidemics on these networks exhibit greater deviations from synthetic models lacking local structure under local interventions(contour plots).
(TIF)

S19 Fig. Personalized PageRank NCP for Mexico City Trace before and after removing a large-sized set of small conductance. The nodes in these deep conductance sets are well separated from the rest of the network.
(TIF)

S20 Fig. College-Penn diffusion data prior to performing sparsification. Epidemic "strength" (original network with no quarantining) varies from $s \approx 3.6$ to $s \approx 324.8$.
(TIF)

S21 Fig. College-Illinois diffusion data prior to performing sparsification. Epidemic "strength" (original network with no quarantining) varies from $s \approx 3.8$ to $s \approx 340$.
(TIF)

S22 Fig. College-Wisc diffusion data prior to performing sparsification. Epidemic "strength" (original network with no quarantining) varies from $s \approx 2.9$ to $s \approx 265.3$.
(TIF)

S23 Fig. The PPR NCP looks characteristically different after sparsifying a network. Panel (A) shows the PPR NCP for Penn94 while (B) shows the PPR NCP after sparsifying. The average degree before and after sparsification is ≈ 65.6 (A) and ≈ 2.9 (B).
(TIF)

S24 Fig. An example that shows the edge swapping procedure for NCP rewiring. We start by picking an edge (u,v) in the graph. Then we pick any two sets S_u and S_v within the NCPs collection of "minimal conductance sets" that contain u and v respectively. Then we find another edge (i,j) that also transits sets S_u and S_v in the same fashion. Rewiring to (u,j) and (v,i) will then preserve the conductance values of S_u and S_v. The downside to this procedure is that it will also alter the conductance values of sets that overlap on any of the nodes involved.
(TIF)

S25 Fig. We study the approximate NCP rewiring as a positive control that to support the idea that local structure drives our findings. For graphs with large AANCP values (Mexico City Trace and LocalGeometric), the approximate NCP rewiring procedure requires more randomization to degrade the impact of interventions on epidemics compared to

configuration model rewiring (Chung-Lu or CL) and Erdős–Rényi (ER). From left to right, we have an example where NCP rewiring roughly preserves the AANCP (Mexico City Trace), an example where it does similar to CL and Erdős–Rényi rewirings (Citation), and an example highlighting what happens with a local geometric model (LocalGeometric). The epidemics parameters for the SEIR models here where chosen to match those in Fig 4. We discuss the rightmost points of the LocalGeometric plot in the text.
(TIF)

S26 Fig. Epidemic NCP plots for extremal CM network variants.
(TIF)

S27 Fig. Epidemic NCP plots for extremal GNP network variants.
(TIF)

S28 Fig. An example of how the AANCP is compute Mexico City Trace. (A) shows the epidemic NCP for Mexico City Trace. (B) computes approximate minimums for this distribution. (C) is a normalized area that is computed from these minimums. When normalizing the size of the set, half the vertices in the graph is set to 1 to handle issues of symmetry.
(TIF)

S29 Fig. The main text uses the Epidemic NCP to display trends between local structure and quarantine impact. Here we display the same trend as in Fig 7 using the Epidemic NCP (left) and personalized PageRank NCP (right). The same broad trend holds. The Spearman ρ correlation coefficient for the personalized PageRank NCP (right) is 0.84 with 95% CI [0.69,0.92]. While this shows a stronger correlation with quarantine impact compared to epidemic NCP, the epidemic NCP is more relevant for epidemic spreading.
(TIF)

S30 Fig. The above supplementary figure shows (leftmost) the epidemic NCP, the personalized PageRank NCP (second from the left) and finally how the susceptible proportion of sets evolves with larger infection probabilities (4 rightmost plots).
(TIF)

S31 Fig The above supplementary figure shows (leftmost) the epidemic NCP, the personalized PageRank NCP (second from the left) and finally how the susceptible proportion of sets evolves with larger infection probabilities (4 rightmost plots).
(TIF)

S32 Fig. The level of granularity composing community structure is relevant for local interventions on epidemic spreading. As we move left to right, the larger communities are composed of aggregated communities from the more granular community structure. As communities become larger, local interventions become less effective. Simulations are SEIR epidemics with $\beta = 0.06$ and $\gamma = 0.05$.
(TIF)

S33 Fig. Multiscale structure alone is insufficient to capture the type of structure we study. Above is the epidemic NCP of a network with multiscale structure using a nested Stochastic Block Model as described in [19]. While this specific model exhibits multiscale structure, this above NCP does not align with empirical NCP measurements characterized as initially-downward-sloping, then upward-sloping, lower-envelope, as the cluster size increases [13,26]. The above is more akin to synthetic geometric network but with oscillatory behavior for each planted block.
(TIF)

Author contributions

Conceptualization: Omar Eldaghar, Michael W. Mahoney, David F. Gleich.

Data curation: Omar Eldaghar, David F. Gleich.

Formal analysis: Omar Eldaghar, Michael W. Mahoney, David F. Gleich.

Funding acquisition: Omar Eldaghar, Michael W. Mahoney, David F. Gleich.

Investigation: Omar Eldaghar, Michael W. Mahoney, David F. Gleich.

Methodology: Omar Eldaghar, David F. Gleich.

Project administration: Omar Eldaghar, Michael W. Mahoney, David F. Gleich.

Resources: Michael W. Mahoney, David F. Gleich.

Software: Omar Eldaghar, David F. Gleich.

Supervision: Michael W. Mahoney, David F. Gleich.

Validation: Omar Eldaghar, Michael W. Mahoney, David F. Gleich.

Visualization: Omar Eldaghar, David F. Gleich.

Writing – original draft: Omar Eldaghar, Michael W. Mahoney, David F. Gleich.

Writing – review & editing: Omar Eldaghar, Michael W. Mahoney, David F. Gleich.

References

1. Kermack WO, McKendrick AG. A contribution to the mathematical theory of epidemics. Proc R Soc Lond Ser A. 1927;115(772):700–21. https://doi.org/10.1098/rspa.1927.0118
2. Apolloni A, Poletto C, Ramasco JJ, Jensen P, Colizza V. Metapopulation epidemic models with heterogeneous mixing and travel behaviour. Theor Biol Med Model. 2014;11:3. https://doi.org/10.1186/1742-4682-11-3 PMID: 24418011
3. Allen LJS. A primer on stochastic epidemic models: formulation, numerical simulation, and analysis. Infect Dis Model. 2017;2(2):128–42. https://doi.org/10.1016/j.idm.2017.03.001 PMID: 29928733
4. Zhang S, Ponce J, Zhang Z, Lin G, Karniadakis G. An integrated framework for building trustworthy data-driven epidemiological models: application to the COVID-19 outbreak in New York City. PLoS Comput Biol. 2021;17(9):e1009334. https://doi.org/10.1371/journal.pcbi.1009334 PMID: 34495965
5. Chang S, Pierson E, Koh PW, Gerardin J, Redbird B, Grusky D, et al. Mobility network models of COVID-19 explain inequities and inform reopening. Nature. 2021;589(7840):82–7. https://doi.org/10.1038/s41586-020-2923-3 PMID: 33171481
6. Le Lay J, Augusto V, Xie X, Alfonso-Lizarazo E, Bongue B, Celarier T, et al. Impact of covid-19 epidemics on bed requirements in a healthcare center using data-driven discrete-event simulation. 2020 Winter Simulation Conference (WSC). IEEE; 2020. p. 771–81.
7. Hunter E, Mac Namee B, Kelleher JD. A comparison of agent-based models and equation based models for infectious disease epidemiology. AICS; 2018. p. 33–44.
8. Bruch E, Atwell J. Agent-based models in empirical social research. Sociol Methods Res. 2015;44(2):186–221. https://doi.org/10.1177/0049124113506405 PMID: 25983351
9. Truszkowska A, Behring B, Hasanyan J, Zino L, Butail S, Caroppo E, et al. High-resolution agent-based modeling of COVID-19 spreading in a small town. Adv Theory Simul. 2021;4(3):2000277. https://doi.org/10.1002/adts.202000277 PMID: 33786413
10. Wilson EB, Worcester J. The law of mass action in epidemiology. Proc Natl Acad Sci U S A. 1945;31(1):24–34. https://doi.org/10.1073/pnas.31.1.24 PMID: 16588678
11. Keeling MJ, Eames KTD. Networks and epidemic models. J R Soc Interface. 2005;2(4):295–307. https://doi.org/10.1098/rsif.2005.0051 PMID: 16849187
12. Costa LdF, Rodrigues FA, Travieso G, Villas Boas PR. Characterization of complex networks: a survey of measurements. Adv Phys. 2007;56(1):167–242. https://doi.org/10.1080/00018730601170527
13. Leskovec J, Lang KJ, Dasgupta A, Mahoney MW. Community structure in large networks: natural cluster sizes and the absence of large well-defined clusters. Internet Math. 2009;6(1):29–123. https://doi.org/10.1080/15427951.2009.10129177
14. Pastor-Satorras R, Castellano C. Distinct types of eigenvector localization in networks. Sci Rep. 2016;6:18847. https://doi.org/10.1038/srep18847 PMID: 26754565

15. Freitas S, Yang D, Kumar S, Tong H, Chau DH. Graph vulnerability and robustness: a survey. IEEE Trans Knowl Data Eng. 2022:1–1. https://doi.org/10.1109/tkde.2022.3163672
16. Allard A, Moore C, Scarpino SV, Althouse BM, Hébert-Dufresne L. The role of directionality, heterogeneity and correlations in epidemic risk and spread. arXiv:200511283 [Preprint]. 2020.
17. Hébert-Dufresne L, Althouse BM, Scarpino SV, Allard A. Beyond R0: heterogeneity in secondary infections and probabilistic epidemic forecasting. J R Soc Interface. 2020;17(172):20200393. https://doi.org/10.1098/rsif.2020.0393 PMID: 33143594
18. Großmann G, Backenköhler M, Wolf V. Heterogeneity matters: contact structure and individual variation shape epidemic dynamics. PLoS One. 2021;16(7):e0250050. https://doi.org/10.1371/journal.pone.0250050 PMID: 34283842
19. Watts DJ, Muhamad R, Medina DC, Dodds PS. Multiscale, resurgent epidemics in a hierarchical metapopulation model. Proc Natl Acad Sci U S A. 2005;102(32):11157–62. https://doi.org/10.1073/pnas.0501226102 PMID: 16055564
20. Balcan D, Colizza V, Gonçalves B, Hu H, Ramasco JJ, Vespignani A. Multiscale mobility networks and the spatial spreading of infectious diseases. Proc Natl Acad Sci U S A. 2009;106(51):21484–9. https://doi.org/10.1073/pnas.0906910106 PMID: 20018697
21. Granovetter MS. The strength of weak ties. Am J Sociol. 1973;78(6):1360–80. https://doi.org/10.1086/225469
22. Watts DJ, Strogatz SH. Collective dynamics of "small-world" networks. Nature. 1998;393(6684):440–2. https://doi.org/10.1038/30918 PMID: 9623998
23. Arenas A, Fernández A, Gómez S. Analysis of the structure of complex networks at different resolution levels. New J Phys. 2008;10(5):053039. https://doi.org/10.1088/1367-2630/10/5/053039
24. Newman MEJ. Modularity and community structure in networks. Proc Natl Acad Sci U S A. 2006;103(23):8577–82. https://doi.org/10.1073/pnas.0601602103 PMID: 16723398
25. Lancichinetti A, Fortunato S. Limits of modularity maximization in community detection. Phys Rev E Stat Nonlin Soft Matter Phys. 2011;84(6 Pt 2):066122. https://doi.org/10.1103/PhysRevE.84.066122 PMID: 22304170
26. Jeub LGS, Balachandran P, Porter MA, Mucha PJ, Mahoney MW. Think locally, act locally: detection of small, medium-sized, and large communities in large networks. Phys Rev E Stat Nonlin Soft Matter Phys. 2015;91(1):012821. https://doi.org/10.1103/PhysRevE.91.012821 PMID: 25679670
27. de Anda-Jáuregui G, Guzmán P, Hernández-Rosales M. The contact network of Mexico City. arXiv:200714596 [Preprint]. 2020.
28. Wang L, Li X. Spatial epidemiology of networked metapopulation: an overview. Chin Sci Bull. 2014;59(28):3511–22. https://doi.org/10.1007/s11434-014-0499-8 PMID: 32214746
29. Soriano-Paños D, Cota W, Ferreira SC, Ghoshal G, Arenas A, Gómez-Gardeñes J. Modeling communicable diseases, human mobility, and epidemics: a review. Ann Phys. 2022;534(6):2100482. https://doi.org/10.1002/andp.202100482
30. Lang JC, De Sterck H, Kaiser JL, Miller JC. Analytic models for SIR disease spread on random spatial networks. J Complex Netw. 2018;6(6):948–70. https://doi.org/10.1093/comnet/cny004
31. Gross B, Havlin S. Epidemic spreading and control strategies in spatial modular network. Appl Netw Sci. 2020;5(1):95. https://doi.org/10.1007/s41109-020-00337-4 PMID: 33263074
32. Butler BA, Paré PE. Optimal safety-critical control of epidemics. IEEE Control Syst Lett. 2023;7:1819–24. https://doi.org/10.1109/lcsys.2023.3280116
33. Liu Q-H, Ajelli M, Aleta A, Merler S, Moreno Y, Vespignani A. Measurability of the epidemic reproduction number in data-driven contact networks. Proc Natl Acad Sci U S A. 2018;115(50):12680–5. https://doi.org/10.1073/pnas.1811115115 PMID: 30463945
34. Hota AR, Godbole J, Pare PE. A closed-loop framework for inference, prediction, and control of SIR epidemics on networks. IEEE Trans Netw Sci Eng. 2021;8(3):2262–78. https://doi.org/10.1109/tnse.2021.3085866
35. Kang Y, Gao S, Liang Y, Li M, Kruse J. Multiscale dynamic human mobility flow dataset in the U.S. during the COVID-19 epidemic. Sci Data. 2020:1–13.
36. Wang B, Gou M, Guo Y, Tanaka G, Han Y. Network structure-based interventions on spatial spread of epidemics in metapopulation networks. Phys Rev E. 2020;102(6–1):062306. https://doi.org/10.1103/PhysRevE.102.062306 PMID: 33466001
37. Keeling MJ, Danon L, Vernon MC, House TA. Individual identity and movement networks for disease metapopulations. Proc Natl Acad Sci U S A. 2010;107(19):8866–70. https://doi.org/10.1073/pnas.1000416107 PMID: 20421468
38. Ajelli M, Gonçalves B, Balcan D, Colizza V, Hu H, Ramasco JJ, et al. Comparing large-scale computational approaches to epidemic modeling: agent-based versus structured metapopulation models. BMC Infect Dis. 2010;10:190. https://doi.org/10.1186/1471-2334-10-190 PMID: 20587041
39. Zachreson C, Chang S, Harding N, Prokopenko M. The effects of local homogeneity assumptions in metapopulation models of infectious disease. R Soc Open Sci. 2022;9(7):211919. https://doi.org/10.1098/rsos.211919 PMID: 35845852
40. Chakrabarti D, Wang Y, Wang C, Leskovec J, Faloutsos C. Epidemic thresholds in real networks. ACM Trans Inf Syst Secur. 2008;10(4):1–26. https://doi.org/10.1145/1284680.1284681
41. Prakash BA, Chakrabarti D, Valler NC, Faloutsos M, Faloutsos C. Threshold conditions for arbitrary cascade models on arbitrary networks. Knowl Inf Syst. 2012;33(3):549–75. https://doi.org/10.1007/s10115-012-0520-y

42. Kiss IZ, Miller JC, Simon PL, et al. Mathematics of epidemics on networks. Cham: Springer; 2017.
43. Tong H, Prakash BA, Tsourakakis C, Eliassi-Rad T, Faloutsos C, Chau DH. On the vulnerability of large graphs. 2010 IEEE International Conference on Data Mining. IEEE; 2010. p. 1091–6.
44. Saha S, Adiga A, Prakash BA, Vullikanti AKS. Approximation algorithms for reducing the spectral radius to control epidemic spread. Proceedings of the 2015 SIAM International Conference on Data Mining. SIAM; 2015. p. 568–76.
45. Chen C, Tong H, Prakash BA, Tsourakakis CE, Eliassi-Rad T, Faloutsos C, et al. Node immunization on large graphs: theory and algorithms. IEEE Trans Knowl Data Eng. 2016;28(1):113–26. https://doi.org/10.1109/tkde.2015.2465378
46. Cucuringu M, Mahoney MW. Localization on low-order eigenvectors of data matrices. arXiv:11091355 [Preprint]. 2011.
47. Salathé M, Jones JH. Dynamics and control of diseases in networks with community structure. PLoS Comput Biol. 2010;6(4):e1000736. https://doi.org/10.1371/journal.pcbi.1000736 PMID: 20386735
48. Liu T, Li P, Chen Y, Zhang J. Community size effects on epidemic spreading in multiplex social networks. PLoS One. 2016;11(3):e0152021. https://doi.org/10.1371/journal.pone.0152021 PMID: 27007112
49. Badham J, Stocker R. The impact of network clustering and assortativity on epidemic behaviour. Theor Popul Biol. 2010;77(1):71–5. https://doi.org/10.1016/j.tpb.2009.11.003 PMID: 19948179
50. Thomas LJ, Huang P, Yin F, Luo XI, Almquist ZW, Hipp JR, et al. Spatial heterogeneity can lead to substantial local variations in COVID-19 timing and severity. Proc Natl Acad Sci U S A. 2020;117(39):24180–7. https://doi.org/10.1073/pnas.2011656117 PMID: 32913057
51. Nowzari C, Preciado VM, Pappas GJ. Analysis and control of epidemics: a survey of spreading processes on complex networks. IEEE Control Syst Mag. 2016;36(1):26–46.
52. Preciado VM, Zargham M, Enyioha C, Jadbabaie A, Pappas G. Optimal resource allocation for network protection: a geometric programming approach. IEEE Trans Control Netw Syst. 2014;1(1):99–108.
53. Mubarak M, Berneburg J, Nowzari C. Individual non-pharmaceutical intervention strategies for stochastic networked epidemics. 2022 IEEE 61st Conference on Decision and Control (CDC). IEEE; 2022. p. 5627–32.
54. Mubarak M, Nowzari C. An agent-based distributed control policy for networked sir epidemics. arXiv:220906250 [Preprint]. 2022.
55. Eshghi S, Khouzani MHR, Sarkar S, Venkatesh SS. Optimal patching in clustered malware epidemics. IEEE/ACM Trans Netw. 2016;24(1):283–98. https://doi.org/10.1109/tnet.2014.2364034
56. Lorch L, De A, Bhatt S, Trouleau W, Upadhyay U, Gomez-Rodriguez M. Stochastic optimal control of epidemic processes in networks. arXiv:181013043 [Preprint]. 2018.
57. Gong K, Tang M, Hui PM, Zhang HF, Younghae D, Lai Y-C. An efficient immunization strategy for community networks. PLoS One. 2013;8(12):e83489. https://doi.org/10.1371/journal.pone.0083489 PMID: 24376708
58. Taghavian F, Salehi M, Teimouri M. A local immunization strategy for networks with overlapping community structure. Phys A: Stat Mech Appl. 2017;467:148–56. https://doi.org/10.1016/j.physa.2016.10.014
59. Hébert-Dufresne L, Allard A, Young J-G, Dubé LJ. Global efficiency of local immunization on complex networks. Sci Rep. 2013;3:2171. https://doi.org/10.1038/srep02171 PMID: 23842121
60. Gupta N, Singh A, Cherifi H. Centrality measures for networks with community structure. Phys A: Stat Mech Appl. 2016;452:46–59. https://doi.org/10.1016/j.physa.2016.01.066
61. Kumar M, Singh A, Cherifi H. An efficient immunization strategy using overlapping nodes and its neighborhoods. Companion Proceedings of the The Web Conference 2018; 2018. p. 1269–1275.
62. Sah P, Leu ST, Cross PC, Hudson PJ, Bansal S. Unraveling the disease consequences and mechanisms of modular structure in animal social networks. Proc Natl Acad Sci U S A. 2017;114(16):4165–70. https://doi.org/10.1073/pnas.1613616114 PMID: 28373567
63. Gosak M, Duh M, Markovič R, Perc M. Community lockdowns in social networks hardly mitigate epidemic spreading. New J Phys. 2021;23(4):043039. https://doi.org/10.1088/1367-2630/abf459
64. Stegehuis C, van der Hofstad R, van Leeuwaarden JSH. Epidemic spreading on complex networks with community structures. Sci Rep. 2016;6:29748. https://doi.org/10.1038/srep29748 PMID: 27440176
65. Min Y, Jin X, Ge Y, Chang J. The role of community mixing styles in shaping epidemic behaviors in weighted networks. PLoS One. 2013;8(2):e57100. https://doi.org/10.1371/journal.pone.0057100 PMID: 23437321
66. Dash Nelson G, Rae A. An Economic geography of the United States: from commutes to megaregions. PLoS One. 2016;11(11):e0166083. https://doi.org/10.1371/journal.pone.0166083 PMID: 27902707
67. Traud AL, Mucha PJ, Porter MA. Social structure of Facebook networks. Phys A: Stat Mech Appl. 2012;391(16):4165–80. https://doi.org/10.1016/j.physa.2011.12.021
68. Leskovec J, Kleinberg J, Faloutsos C. Graphs over time: densification laws, shrinking diameters and possible explanations. Proceedings of the Eleventh ACM SIGKDD International Conference on Knowledge Discovery in Data Mining; 2005. p. 177–87.
69. Gehrke J, Ginsparg P, Kleinberg J. Overview of the 2003 KDD Cup. SIGKDD Explor Newsl. 2003;5(2):149–51. https://doi.org/10.1145/980972.980992

70. Boldi P, Rosa M, Santini M, Vigna S. Layered label propagation: a multiresolution coordinate-free ordering for compressing social networks. Proceedings of the 20th WWW2011; 2011. p. 587–96.
71. Cho E, Myers SA, Leskovec J. Friendship and mobility: user movement in location-based social networks. Proceedings of the 17th ACM SIGKDD International Conference on Knowledge Discovery and Data Mining; 2011. p. 1082–90.
72. Leskovec J, Krevl A. SNAP datasets: Stanford large network dataset collection; 2014. Available from: http://snap.stanford.edu/data
73. Klimt B, Yang Y. Introducing the Enron corpus. CEAS. vol. 45; 2004. p. 92–6.
74. Leskovec J, Kleinberg J, Faloutsos C. Graph evolution: densification and shrinking diameters. ACM Trans Knowl Discov Data. 2007;1(1):2-es.
75. Richardson M, Agrawal R, Domingos P. Trust management for the semantic web. The Semantic Web-ISWC 2003: Second International Semantic Web Conference; 2003 Oct 20–23; Sanibel Island, FL, USA. Proceedings 2. Springer; 2003. p. 351–68.
76. Wilson C, Boe B, Sala A, Puttaswamy KPN, Zhao BY. User interactions in social networks and their implications. Proceedings of the 4th ACM European conference on Computer systems. EuroSys '09. New York, NY, USA: ACM; 2009. p. 205–18.
77. Mislove A, Marcon M, Gummadi KP, Druschel P, Bhattacharjee B. Measurement and analysis of online social networks. Proceedings of the 7th ACM SIGCOMM Conference on Internet Measurement. IMC '07. New York, NY, USA: ACM; 2007. p. 29–42.
78. Veldt N, Gleich D, Wirth A. Learning resolution parameters for graph clustering. The World Wide Web Conference; 2019. p. 1909–19.
79. Cohen R, Havlin S, Ben-Avraham D. Efficient immunization strategies for computer networks and populations. Phys Rev Lett. 2003;91(24):247901. https://doi.org/10.1103/PhysRevLett.91.247901 PMID: 14683159
80. Gleich DF, Seshadhri C. Vertex neighborhoods, low conductance cuts, and good seeds for local community methods. KDD2012; 2012. p. 597–605.
81. Fountoulakis K, Liu M, Gleich DF, Mahoney MW. Flow-based algorithms for improving clusters: a unifying framework, software, and performance. SIAM Rev. 2023;65(1):59–143. https://doi.org/10.1137/20m1333055
82. Adcock AB, Sullivan BD, Mahoney MW. Tree-like structure in large social and information networks. Proc. of the 2013 IEEE ICDM; 2013. p. 1–10.
83. Adcock AB, Sullivan BD, Mahoney MW. Tree decompositions and social graphs. Internet Math. 2016;12(5):315–61. https://doi.org/10.1080/15427951.2016.1182952
84. Andersen R, Chung F, Lang K. Local graph partitioning using pagerank vectors. 2006 47th Annual IEEE Symposium on Foundations of Computer Science (FOCS'06). IEEE; 2006. p. 475–86.
85. Goltsev AV, Dorogovtsev SN, Oliveira JG, Mendes JFF. Localization and spreading of diseases in complex networks. Phys Rev Lett. 2012;109(12):128702. https://doi.org/10.1103/PhysRevLett.109.128702 PMID: 23006000
86. Pastor-Satorras R, Castellano C. Eigenvector localization in real networks and its implications for epidemic spreading. J Stat Phys. 2018;173(3–4):1110–23. https://doi.org/10.1007/s10955-018-1970-8
87. Gleich DF, Kloster K. Seeded PageRank solution paths. Eur J Appl Math. 2016;27(6):812–45.
88. Ghalmane Z, Hassouni ME, Cherifi H. Immunization of networks with non-overlapping community structure. Soc Netw Anal Min. 2019;9(1):1–22. https://doi.org/10.1007/s13278-019-0591-9
89. Eckles D, Mossel E, Rahimian MA, Sen S. Long ties accelerate noisy threshold-based contagions. arXiv:181003579 [Preprint]. 2018.
90. Onnela J-P, Saramäki J, Hyvönen J, Szabó G, Lazer D, Kaski K, et al. Structure and tie strengths in mobile communication networks. Proc Natl Acad Sci U S A. 2007;104(18):7332–6. https://doi.org/10.1073/pnas.0610245104 PMID: 17456605
91. Borgatti SP, Everett MG. Models of core/periphery structures. Soc Netw. 2000;21(4):375–95. https://doi.org/10.1016/s0378-8733(99)00019-2
92. Mercier A, Scarpino S, Moore C. Effective resistance against pandemics: mobility network sparsification for high-fidelity epidemic simulations. PLoS Comput Biol. 2022;18(11):e1010650. https://doi.org/10.1371/journal.pcbi.1010650 PMID: 36413581
93. Wren L, Best A. How local interactions impact the dynamics of an epidemic. Bull Math Biol. 2021;83(12):124. https://doi.org/10.1007/s11538-021-00961-w PMID: 34773169
94. Cushing JM, Yicang Z. The net reproductive value and stability in matrix population models. Nat Resour Model. 1994;8(4):297–333. https://doi.org/10.1111/j.1939-7445.1994.tb00188.x
95. Miller JC. Spread of infectious disease through clustered populations. J R Soc Interface. 2009;6(41):1121–34. https://doi.org/10.1098/rsif.2008.0524 PMID: 19324673
96. Silva DH, Ferreira SC. Dissecting localization phenomena of dynamical processes on networks. J Phys Complex. 2021;2(2):025011. https://doi.org/10.1088/2632-072x/abdd98
97. Gross T, D'Lima CJD, Blasius B. Epidemic dynamics on an adaptive network. Phys Rev Lett. 2006;96(20):208701. https://doi.org/10.1103/PhysRevLett.96.208701 PMID: 16803215
98. Gates MC, Woolhouse MEJ. Controlling infectious disease through the targeted manipulation of contact network structure. Epidemics. 2015;12:11–9. https://doi.org/10.1016/j.epidem.2015.02.008 PMID: 26342238
99. Grange ZL, Goldstein T, Johnson CK, Anthony S, Gilardi K, Daszak P, et al. Ranking the risk of animal-to-human spillover for newly discovered viruses. Proc Natl Acad Sci U S A. 2021;118(15):e2002324118. https://doi.org/10.1073/pnas.2002324118 PMID: 33822740
100. Sánchez CA, Li H, Phelps KL, Zambrana-Torrelio C, Wang L-F, Zhou P, et al. A strategy to assess spillover risk of bat SARS-related coronaviruses in Southeast Asia. Nat Commun. 2022;13(1):4380. https://doi.org/10.1038/s41467-022-31860-w PMID: 35945197